Activation of the cognitive control network associated with information uncertainty

Tingting Wu[a], **Kurt P. Schulz**[b], **Jin Fan**[a,*]

[a]Department of Psychology, Queens College, The City University of New York, Queens, NY, USA

[b]Department of Psychiatry, Icahn School of Medicine at Mount Sinai, New York, NY, USA

Abstract

The cognitive control network (CCN) that comprises regions of the frontoparietal network, the cingulo-opercular network, and other sub-cortical regions as core structures is commonly activated by events with an increase in information uncertainty. However, it is not clear whether this CCN activation is associated with both information entropy that represents the information conveyed by the context formed by a sequence of events and the surprise that quantifies the information conveyed by a specific type of event in the context. We manipulated entropy and surprise in this functional magnetic resonance imaging study by varying the probability of occurrence of two types of events in both the visual and auditory modalities and measured brain response as a function of entropy and surprise. We found that activation in regions of the CCN increased as a function of entropy and surprise in both the visual and auditory tasks. The frontoparietal network and additional structures in the CCN mediated the relationship between these information measures and behavioral response. These results suggest that the CCN is a high-level modality-general neural entity for the control of the processing of information conveyed by both context and event.

Keywords

Cognitive control; Cognitive control network; Entropy; Surprise; Uncertainty

1. Introduction

Cognitive control is the process that coordinates thoughts and actions under conditions of uncertainty (Fan, 2014; Miller and Cohen, 2001; Posner and Snyder, 1975). A large-scale brain network, the cognitive control network (CCN), shows a general and reliable involvement in cognitive control across different tasks in various domains (Cai et al., 2014; Derrfuss et al., 2005; Fan et al., 2014; Nee et al., 2007; Niendam et al., 2012; Wu et al., 2019a). The CCN consists of two subnetworks, the frontoparietal network (FPN) comprised of the frontal eye field (FEF) and the areas near and along the intraparietal sulcus (IPS) (Corbetta, 1998; Fan, 2014), and the cingulo-opercular network (CON) with the anterior cingulate cortex (ACC) and the anterior insular cortex (AIC) as the two key structures (Dosenbach et al., 2008; Dosenbach et al., 2007), as well as subcortical structures including the thalamus and the basal ganglia (Fan, 2014; Koziol, 2014; Rossi et al., 2009; Wu et al., 2019a). Although activation of the CCN has been attributed to the event-related flanker conflict effect (e.g., Fan et al., 2003; Lau et al., 2006; Luks et al., 2007) and explained by the models of conflict monitoring and resolution (Botvinick et al., 1999; Botvinick et al., 2001; Braver et al., 2001; Carter et al., 1998. 2000; MacDonald et al., 2000; Posner and DiGirolamo, 1998), the general function of the CCN in cognitive control is still not fully understood because these models cannot account for activation of the CCN in the absence of conflict (see Fan, 2014 for a review).

We have proposed an information theory account of cognitive control that explains the CCN as a high-level entity for the control of uncertainty processing even in the absence of explicit conflict (Fan, 2014). According to this account, the CCN tracks the level of uncertainty. Uncertainty can be engendered by a context composed of a set of events (e.g., a sequence of symbols) and a single event type (e.g., a single type of symbol in a sequence), with more unpredictable and less deterministic context or low frequency events conveying a greater amount of information. The amount of information, i.e., the level of uncertainty, can be quantified based on information theory (Shannon and Weaver, 1949). Specifically, the uncertainty of a context (X) that is comprised of n possible types of events of $\{x_1 \ldots x_n\}$ can be quantified as *information entropy* (H) in unit of bits as $H(X) = -\sum_{i=1}^{n} p(x_i)\log_2 p(x_i)$, where $p(x_i)$ is the probability of event type x_i. The unit of bits is based on the use of the binary logarithm (i.e., 0 versus 1) to encode information. A high information entropy value indicates greater unpredictability of the context. For example, a series of repeating left-pointing (L) arrows for left response with no right-pointing (R) arrows for right response ("LLLLLLLLLL", in which $p_L = 100\%$ and $p_R = 0\%$) has an entropy value of 0 bit, because the sequence is totally predictable. In contrast, a random sequence of left-pointing and right-pointing arrows presented in equal probability ("LRLLRRLRLR", in which $p_L = p_R = 50\%$) has the highest entropy value of 1 bit because the sequence is not predictable. The information conveyed by the occurrence of each single event type x_i can be quantified as *surprise* (I) in bits as $I(x_i) = -\log_2 p(x_i)$, with a low probability event type carrying a greater amount of information. For any two types of events presented with different frequencies in a sequence, the event type with a lower probability of occurrence has a higher surprise value that indicates the event type is more unpredictable. For example, the low-probability

(20%) right-pointing arrows in the sequence "LLLLRLLRLL" has a higher surprise value of 2.32 bits than the high-probability (80%) left-pointing arrows with a surprise value of 0.32 bit. In addition, the dependency between events may provide additional information that can reduce the uncertainty of a context, e.g. a sequence containing a repeating pattern of event occurrence (e.g., "LRLRLRLRLR") is more predictable compared to a random sequence. The amount of information conveyed by the dependency of events can be quantified as mutual information, which is computed based on the formula $M\ I = \sum_{i,j} p_{i,j} \log \frac{p_{i,j}}{p_i p_j}$, where p_i and p_j are the frequencies of event types i and j, and $p_{i,j}$ is the probability that event type j occurs right after event type i. A larger mutual information value indicates greater reduction in the uncertainty of a context due to the dependency between events.

The proposal that the CCN is an information processing entity in the brain for cognitive control would be supported by the evidence that activation of this network increases as a function of amount of information conveyed by the context and event. The role of the CCN in controlling the processing of information conveyed by the context remains elusive. Studies with the context uncertainty quantified in terms of information entropy focused on the contribution of hippocampus to statistical learning processes (e.g., Harrison et al., 2006; Nastase et al., 2014; Strange et al., 2005), rather than the role of the CCN in cognitive control. In addition, existing evidence of the increase in activation of the CCN associated with low-probability events in classical cognitive control tasks suggests that the CCN may play a role in the control of information processing related to a specific event type (see Fan, 2014 for a review). For example, an increase in activation in the CCN is typically observed when contrasting the low-probability No-Go condition to the high-probability Go condition in Go/No-Go tasks in studies of inhibitory control (Braver et al., 2001; Cai et al., 2014; Niendam et al., 2012; Wu et al., 2019a). The activation increase in the CCN may be attributed to the relative increase in surprise for the low-probability No-Go events based on the information theory account of cognitive control although the engagement of inhibitory processing needs to be controlled in order to identify the effect of surprise in terms of the activation of the CCN. Taken together, direct examination of the involvement of the CCN in the processing of information conveyed by context and event has heuristic value for understanding the functional property of the CCN in relation to information entropy and surprise. Recruitment of the CCN to process information inputs from different sensory modalities (e.g., visual and auditory) would provide evidence for a general role of the CCN in cognitive control independent of modality, i.e., supra-modal (Spagna et al., 2015, 2020; Wu et al., 2020). Evidence that CCN activation mediates the relationship between the information amount and the behavioral performance would inform us about how the brain implements cognitive control to coordinate thoughts (uncertainty representation and resolution) and actions (motor generation) under uncertainty (as in Wu et al., 2018).

Information entropy and surprise were manipulated in this functional magnetic imaging (fMRI) study by varying the probability of two types of events in a sequence in separate visual and auditory tasks presented in two separate experiments. The association between activation in regions of the CCN and information entropy and surprise was examined in each task for evidence of the involvement of the CCN in the processing of context and event, respectively. The role of the CCN in the processing of uncertainty was further examined

by testing whether the activation of the CCN mediates the relationship between information entropy (and surprise) and behavioral performance (in terms of reaction time, RT). The parallel design of the visual and the auditory versions of the task allowed us to test the hypothesis that the CCN supports cognitive control for high-level abstract information independent of input modality.

2. Methods

2.1. Participants

A total of 58 adult volunteers participated in this study. Data from 11 participants were excluded from the analysis due to the diagnosis of a neural abnormality (e.g., increased density in gray matter) in the anatomical scans by an attending neuroradiologist ($n = 4$); failure to complete the tasks ($n = 4$); excessive head motion (movement > 10 mm) ($n = 2$); and low overall mean accuracy (< 75%) ($n = 1$). The final sample consisted of 47 participants, including 35 who participated in the visual experiment (19 females and 16 males; mean ± standard deviation (SD) age = 28.3 ± 5.2 years, range = 22–39 years) and 35 who participated in the auditory experiment (21 females and 14 males, mean ± SD age = 26.7 ± 5.0, range: 19–39 years), with 23 who participated in both experiments during separate visits. None of the final participants reported a history of head injury nor a history of psychiatric or neurological disorders. This study was approved by the institutional review boards of The City University of New York and the Icahn School of Medicine at Mount Sinai (ISMMS). Written informed consent was obtained from all participants. Participants were compensated for their participation in the study.

2.2. Uncertainty Variation Tasks (UVTs)

The uncertainty variation tasks (UVTs) were developed to parametrically manipulate the level of uncertainty in information entropy and surprise by varying the probability of binary choices in a sequence of trials. Each event in the visual version of the UVT (UVT-V) began with a fixation period jittered from 0 to 0.5 s (uniformly distributed), followed by the presentation of a left- or right-pointing arrow (length = 0.52° in visual angle) as the stimulus of interest in one of eight possible locations equidistant (1.2°) from the central fixation cross. Participants were instructed to indicate the direction of the arrow by pressing the corresponding button as quickly and accurately as possible. The arrow disappeared once a response was received or after 1.5 s if no response was recorded within this response window. Each event lasted 2 s in total.

The UVT-V consisted of eight 346-s runs that all began and ended with a 30 s period of fixation. Each run consisted of 128 stimuli that were organized into four 32-stimulus blocks separated by three 10-s inter-block fixation periods. The probability of each of the two possible arrow directions (left-pointing: L; right-pointing: R) was manipulated across these four blocks (sequences) to create four block types (Table 1): (1) all 32 arrows presented in the same direction (Constant block, e.g., LLLLLL…, probability of two direction = 100% versus 0%); (2) two directions alternating (Alternating block, e.g. LRLRLR …); (3) 28 arrows in one direction (high-probability trial, probability = 87.5%) mixed with 4 arrows in the other direction (low-probability trial, probability = 12.5%) presented in random order

(the Unbalanced block); and (4) 16 arrows in each direction presented in random order (Balanced block, probability of each direction = 50%). Fig. 1a illustrates a partial sequence (8 out of 24 stimuli) of the Balanced block of the UVT-V. Participants were explicitly instructed about the four types of blocks before performing the task. The order of the blocks was counterbalanced using a Latin-squares design and the same sequence of blocks was used for all participants to avoid systematic impacts of signal drifting and fatigue across time. There were a total 256 arrows (stimuli) for each of the Constant, Alternating, Unbalanced, and Balanced blocks, including 224 high-probability and 32 low-probability stimuli for the Unbalanced block type. The entire task consisted of 32 blocks (1024 stimuli) that lasted approximately 50 min.

The design of the auditory version of the UVT (UVT-A) was identical to the UVT-V, with the arrows replaced by auditory tones of 200 ms duration (gated on and off with 15 ms cosine ramps to reduce audible clicks). The auditory stimuli consisted of eight low-pitched tones with frequencies ranging from 400 Hz to 484 Hz (400, 412, 424, 436, 448, 460, 472, and 484 Hz) and eight high-pitched tones with frequencies ranging from 1016 Hz to 1100 Hz (1016, 1028, 1040, 1052, 1064, 1076, 1088, and 1100 Hz). The tones were presented in a diotic manner at an intensity that was comfortable for the participant and clearly audible over the background scanner noise. Fig. 1b illustrates a partial sequence (8 out of 24 events) in the Balanced block of the UVT-A. Participants were instructed to indicate whether each tone was a low-pitched or high-pitched tone by pressing the corresponding response button.

The target location in the UVT-V and tone frequency in the UVT-A were varied to avoid (1) overlap of target locations and frequencies on consecutive stimuli to clearly separate the stimuli in a sequence; and (2) habituation to the repeated stimuli and loss of attention to the task. These variations were orthogonal to the manipulation of the probability of event type, and resulted in a constant increase in baseline uncertainty across all stimuli termed the state uncertainty (Fan et al., 2014).

2.3. fMRI data acquisition

Participants were scanned on a 3 T Siemens Allegra MRI system with a 16-channel phase-array coil (Siemens, Erlangen, Germany) at ISMMS. All images were acquired along axial parallel to the anterior commissure-posterior commissure (AC-PC) plane. Eight runs of 139 $T2^*$-weighted gradient-echo echo-planar imaging (EPI) images were acquired during each task with repetition time (TR) = 2500 ms, echo time (TE) = 27 ms, flip angle = 82°, field of view (FOV) = 240 mm, matrix size = 64 × 64, voxel size = 3.75 × 3.75 × 4 mm, and 40 axial slices of 4 mm thickness with no skip. Two additional images at the beginning of each run were discarded to allow for equilibration of T1 saturation effects. A T2-weighted anatomical volume of the whole brain was acquired using a turbo spin-echo pulse sequence (TR = 4050 ms, TE = 99 ms, flip angle = 170°, FOV = 240 mm, matrix size = 448 × 512, voxel size = 0.47 × 0.47 × 4 mm, 40 axial slices of 4 mm thickness with no skip). The entire scan session lasted approximately 1 h.

2.4. Procedure

The tasks were compiled and run using E-Prime software (RRID: SCR_009567; Psychology Software Tools, Pittsburgh, PA). Participants practiced one run of the task on a desktop PC before the scan. They were guided to differentiate the four block types during the training. Visual stimuli for the actual scan were projected using a liquid crystal display projector onto a screen mounted at the back of the magnet bore with a viewing distance of 55 cm. Auditory stimuli in the UVT-A were presented in both ears via an MRI-compatible headphone. Participants responded to each trial by pressing the buttons with their right index finger and right middle fingers to indicate "left" and "right" pointing directions, respectively, in visual task and "low-pitched" and "high-pitched" tones, respectively, in the auditory task, using an MRI-compatible fiber optic button system (5-Button Right response unit, BrainLogic, PST Inc.).

2.5. Estimation of uncertainty based on information theory and analytic outline

Below we used p_1 and p_2 to refer to the probabilities of two event types. The four task blocks of sequences in each task were treated as four different contexts (Table 1): Constant ($p_1 = 100\%$, $p_2 = 0\%$), Alternating ($p_1 = p_2 = 50\%$, with a fixed alternating order of stimulus presentation), Unbalanced ($p_1 = 87.5\%$, $p_2 = 12.5\%$, with a random order of stimulus presentation), and Balanced ($p_1 = p_2 = 50\%$, with a random order of stimulus presentation). The effect of uncertainty conveyed by the context was examined to test the effect of entropy by comparing the Constant, Unbalanced, and Balanced blocks types. The information entropy value (H) was 0 bit for the Constant block [$-1 \times \log_2 (1) - 0 \times \log_2 (0) = 0$], 0.54 bit for the Unbalanced block [$-0.875 \times \log_2 (0.875) - 0.125 \times \log_2 (0.125) = 0.54$], and 1 bit for the Balanced block [$-0.5 \times \log_2 (0.5) - 0.5 \times \log_2 (0.5) = 1$]. The Constant block, rather than the Alternating block, was considered as the 0-bit reference condition. Although the Alternating block contained two alternative choices that were completely predictable due to the fixed order of stimulus presentation, analysis of RT revealed that the total amount of information in this block was more than 0 bit (see Results). The Alternating block was only used to examine the activation reduction due to mutual information (see below).

The effect of the increase in uncertainty conveyed by a low probability event was examined by computing the difference in surprise value between the low-probability events and the high-probability events in the context of the Unbalanced block. The surprise value was 3 bits for the low-frequency events [$-\log_2 (0.125) = 3$] and 0.19 bit for the high-frequency events [$-\log_2 (0.875) = 0.19$]. Although the surprise values for events in the other three blocks were also computable, these events were not included in the analysis of the effect of surprise to avoid the confounding effects of entropy and mutual information, which differed between blocks.

The effect of event dependency was examined by comparing mutual information in the Alternating and Balanced blocks, which differed only in predictability of the event type in each stimulus by the previous stimulus (i.e., completely predictable in the Alternating block and completely unpredictable in the Balanced block). The presentation order of the two types of events (coded as 0 and 1) of consecutive stimuli resulted in four possible

combinations: "0, 0" (probability: $p_{0,0}$); "0, 1" (probability: $p_{0,1}$); "1, 0" (probability: $p_{1,0}$); and "1, 1" (probability: $p_{1,1}$). The probability of these combinations of consecutive trials was $p_{0,0} = p_{1,1} = 0$, and $p_{0,1} = p_{1,0} = 0.5$ for the Alternating block and $p_{0,0} = p_{1,1} = p_{0,1} = p_{1,0} = 0.25$ for the Balanced block. Thus, the mutual information was 1 bit for the Alternating block $[2 \times 0 \times \log_2 \frac{0}{0.5 \times 0.5} + 2 \times 0.5 \times \log_2 \frac{0.5}{0.5 \times 0.5} = 1]$ and 0 bit for the Balanced block $[4 \times 0.25 \times \log_2 \frac{0.25}{0.5 \times 0.5} = 0]$.

Behavioral performance and brain responses were compared across blocks to test the effects of information entropy and mutual information, and were compared across event types within the Unbalanced block to examine the effect of surprise (Table 1). Based on previous behavioral and fMRI studies (Hick, 1952; Hyman, 1953; Wu et al., 2018), it was predicted that an increase in information entropy would be associated with a linear increase in both RT and activation in the regions of the CCN. Higher order nonlinear relationships were not examined due to a lack of hypothesis. It was also predicted that an increase in surprise would be associated with monotonic increases in both RT and activation, while an increase in mutual information would be associated with decreases in both RT and activation in the regions of the CCN. The specific forms of these associations (linear versus non-linear) were not examined because both surprise and mutual information were only manipulated between two conditions in the tasks.

2.6. Behavioral data analysis

The error rate and mean RT for each task were first analyzed at the subject level. Trials (stimuli) with no response or incorrect responses were considered errors and were excluded from the calculation of mean RT. Trials with RT exceeding 3 SD of the mean for trials with correct responses in each condition were considered outliers and were also excluded from the analysis of RT (mean ± SD exclusion rate = 0.04 ± 0.1%). The average RT for each condition was calculated across the remaining trials for that condition.

Mean RTs for each condition for each participant were entered into group-level analyses of the effect of uncertainty on RT. Group-level analysis was not conducted on error rate due to a floor effect on both tasks. The mean error rate across all participants was only computed and checked to ensure that participants understood the instruction and successfully completed the tasks with a low error rate. The effects of information entropy, surprise, and mutual information on RT were analyzed separately. The Hick-Hyman law (Hick, 1952; Hyman, 1953) that describes a linear relationship between RT and information entropy was applied to analyze the effect of entropy using the generalized linear mixed effect model (GLMM), with task condition as the fixed effect and participant as the random effect. Here, $RT = b_0 + b_1 H$, in which the H refers to the entropy value in the Constant, Unbalanced, and Balanced blocks (0, 0.54, and 1 bit, respectively); the intercept b_0 was the baseline RT, and the slope b_1 was the cost in RT associated with each bit of increase in information entropy. This GLMM enabled us to test whether the increase in RT was a linear function of entropy (i.e., whether b_1 was significantly greater than 0) and to estimate the slope of the cost in RT as a function of entropy (i.e., the value of b_1). The GLMM were conducted using the *fitlme* function (http://mathwork.com/help/fitlme.html#d120e303009)

in Matlab version R2017b. The cost in RT associated with an increase in surprise was examined by comparing the RT in the low-probability event type versus the high-probability event type in the Unbalanced block using a paired t test (one-tailed), with a prolonged RT predicted in the low-probability event type compared to the high-probability event type.

An increase in dependency between events (i.e., increase in mutual information) would reduce uncertainty of a context associated with a reduction in RT. The reduction in RT associated with each bit of increase in mutual information was examined by comparing the Alternating block versus the Balanced block using a paired t-test, with RT predicted to be shorter in the Alternating block than the Balanced block. The total amount of uncertainty in the Alternating block after information reduction in contrast to the Balanced block was estimated as $(1 - (RT_{Balanced} - RT_{Alternating})/b_1) H_{Balanced}$.

2.7. fMRI data analysis

2.7.1. Image preprocessing—Event-related fMRI data analysis was conducted using the statistical parametric mapping package (SPM 12, RRID: SCR_007037; Welcome Trust Centre for Neuroimaging, London, UK). The T2 and EPI images were manually adjusted to align with the AC-PC plane if necessary. The EPI images of each participant were realigned to the first image of the first run, and slice timing corrected using the first slice of each image as the reference. Realignment residuals were further reduced and bad volumes were detected and repaired using the ArtRepair software (https://cibsr.stanford.edu/tools/human-brain-project/artrepair-software.html; RRID: SCR_005990). The processed EPI images were coregistered to the T2 image, spatially normalized to the SPM T2 template in a standardized space of Montréal Neurological Institute (MNI) ICBM152, and spatially smoothed with a Gaussian kernel of 8 mm full-width half maximum.

2.7.2. General linear modeling—Subject-level general linear modeling (GLM) was conducted to detect the blood-oxygen-level-dependent (BOLD) signals associated with information entropy, surprise, and mutual information for each participant. For each run, a vector of the onsets of arrows (or tones) in stimulus events with correct behavioral responses was constructed for each of the five conditions (the constant, alternating, high-probability, balanced, and low-probability conditions) with the duration of each event as 0. The number of useable events in the low-probability condition was around 30 (88.6% accuracy of the total 32 events), which was considered the minimum to provide sufficient power to detect BOLD signal change. An additional vector for the stimuli in stimulus events with incorrect responses (if any) was constructed for each condition (for a maximum of 5 vectors per run). The vectors were convolved with a standard hemodynamic response function (HRF) (Friston et al., 1998) to generate corresponding regressors for the GLM. The regressors for incorrect responses were treated as nuisance regressors. Nuisance regressors to model head motion using the Friston 24-parametre model (Friston et al., 1996) were also entered, in which each run included 6 head motion parameters of the current volume estimated during realignment, 6 head motion parameters of the preceding volume, and the squared item of each parameter. Low-frequency signal drift in each run was removed using a high-pass filter with a 256-s cutoff. This cutoff value was chosen rather than the default 128-s cutoff

because the tasks were in a mixed event-related and block design with the length of each block equal to 56 s. Serial correlations were estimated with an autoregressive AR(1) model.

Orthogonal polynomial contrasts were applied to the images of parameter estimates to identify brain regions with activation associated with uncertainty. The increase in brain activation as a linear function of information entropy was identified using a contrast vector corresponding to the constant, low-probability, high-probability, and balanced conditions [0, 0.0675, 0.4725, 1]. The contrast values of the low-probability and high-probability conditions in this contrast were computed as the entropy in Unbalanced block (0.54 bit) weighted by their probability (low-probability: $0.54 \times 0.125 = 0.0675$; high-probability: $0.54 \times 0.875 = 0.4725$). This contrast reflects the contribution of these two event types in proportion to the total BOLD signal change associated with the increase in entropy in this condition. This contrast vector was further demeaned to remove the zero-order term and then normalized by dividing by the maximum of the absolute values. The contrast of the low-probability condition *minus* the high-probability condition was used to identify brain regions with an increase in activation associated with an increase in surprise, while the contrast of the alternating condition *minus* the balanced condition was used to identify brain regions with a reduction in activation associated with an increase in mutual information.

For each contrast, the images of contrast estimates for all participants were entered into second-level group analyses conducted with one-sample *t* tests using a random effects model with subject as the random effect. The thresholds for these analyses were set at an uncorrected voxel-wise level of $p < .01$ for the height and a contiguous-voxel thresh-old, *k*, estimated based on random field theory (Friston et al., 1994) for the extent to correct for multiple voxel comparisons at a cluster-level of $p < .05$.

2.7.3.   Regions of interest analysis—A region of interest (ROI) analysis was conducted to illustrate activation in regions of the CCN under different conditions. The independent coordinates of ROIs were defined based on our previous meta-analysis (Wu et al., 2019a): ACC [2, 16, 48], AIC (left [−32, 22, −2], right [34, 22, −2]), FEF (left [−26, −2, 56], right [30, −2, 60]), and IPS (left [−32, −52, 44], right [42, −42, 44]). The first eigenvariate of the beta values was extracted from all voxels within a 6 mm diameter sphere around the ROI coordinates for the contrast image for each of the five conditions versus baseline. Because there was no prior hypothesis of hemispheric specialization in the CCN for cognitive control, activation in each brain region in the two hemispheres was averaged to reduce the number of ROIs for the illustration of the brain activation as a function of uncertainty.

2.7.4.   Single-event brain response extraction—Whole-brain responses to each visual and auditory stimulus in each event were extracted using an "extract-one-event-out" approach (Choi et al., 2012; Kinnison et al., 2012; Rissman et al., 2004; Wu et al., 2018, 2019b). Specifically, a participant-specific GLM were constructed for each event, which consisted of all regressors in the participant-specific GLM described above, except that the regressor for the condition containing the event of interest was split into two regressors: (1) one regressor constructed by the convolution of the vector for the onset of arrow/tone in the event of interest with the standard HRF, which modeled the expected neural responses

associated with this individual event; and (2) one regressor constructed by the convolution of the vector for the onsets of arrows/tones in the rest of events in the same condition, which modeled the expected neural responses associated with events of no interest. The estimation of the event-specific GLM was looped event-by-event across all events with a correct response, resulting in one *beta* image for each event corresponding to the single-event brain response. Trials with global-mean *beta* values greater or less than 3 SD of the mean across all events were considered as outliers and excluded from the following mediation analyses. The detection and estimation power of this single-event brain response extraction approach was demonstrated in our previous study using a similar mixed block and event-related design (Wu et al., 2018).

2.7.5.   Whole-brain voxel-wise multilevel mediation analysis—Brain responses mediating each of the entropy-RT and surprise-RT relationships were identified by multi-level mediation analysis (Atlas et al., 2010, 2014; Wager et al., 2008, 2009) using the mediation toolbox (https://github.com/canlab/MediationToolbox). The initial variable (X) for each mediation model was the measure of uncertainty (entropy or surprise) in bits, the outcome variable (Y) was the RT, and the mediator (M) was the single-event *beta* values of each voxel. Three effects were examined using this mediation model: (1) path a that modeled the effect of uncertainty on brain activation (X to M) to identify brain regions involved in the representation and processing of entropy/surprise, which is equivalent to the GLM; (2) path *b* that modeled the association between brain activation and RT controlling for uncertainty (M to Y controlling X) to identify brain regions involved in response generation; and (3) mediation effect that modeled brain activation mediating the relationship between uncertainty and RT (X to M to Y) to identify brain regions that mediate the representation/processing of uncertainty and response generation. The mediation effect was calculated as the difference between the total effect of X on Y (path *c*, i.e., the association between entropy/surprise and RT examined in behavioral analysis) and the direct effect of X on Y controlling for the M (path *c'*). The mediation effect was estimated in an equivalent manner as the sum of the product of path coefficients $a \times b$ and the covariance between *a* and *b* (MacKinnon et al., 2000), i.e., $c - c' = a \times b + \text{cov}(a, b)$, which measures the amount of covariance between X and Y that can be explained by the M. Mediation analysis was conducted for each voxel, and the voxel-wise coefficient for each effect was estimated for each participant. For each path, the coefficient images from all participants were then entered into the second-level group analysis to identify brain regions with a significant difference from 0 using a random effects model with subject as the random effect. For the second-level group analyses, significance was set at an uncorrected voxel-wise level of $p <$ .001 for the height together with a contiguous-voxel threshold of $k = 50$ for the path *a* and *b*. Because of a priori hypothesis of the CCN acting as the mediator, the significance for the mediation effect was set at a more liberally level with an uncorrected voxel-wise level of $p < .01$ for the height together with a contiguous-voxel threshold of $k = 100$, because of our a priori hypothesis postulating that the CCN acts as the mediator. These contiguous-voxel thresholds were empirically chosen based on previous studies that originally designed and applied the mediation toolbox (Atlas et al., 2010, 2014; Wager et al., 2008, 2009).

3. Results

3.1. Results of behavioral analysis

Mean and variability of RT and error rate for each task condition of the UVT-V and UVT-A are shown in Fig. 2 and Table 2. The variability measure was reported in Fig. 2 using error bars representing 95% confidence intervals of the within-subject design estimated with a within-person centering approach to remove the impact of within-subject variance to facilitate direct comparisons between conditions (Cousineau, 2005). SD was reported in Table 2 to reflect individual differences in each condition. The error rate was low (< 5%) in all task conditions except for the low-probability condition of the UVT-V (11.4%). RT varied as a linear function of information entropy in both tasks, with the slope of each fitted linear function significantly greater than 0 (UVT-V: RT = 454.4 + 88.4H. slope: $F_{1, 68.78}$ = 43.73, p < .001; UVT-A: RT = 494.9 + 98.6 H. slope: $F_{1, 68.65}$ = 15.88, p < .001). A significant increase in RT due to an increase in surprise was revealed in both tasks (UVT-V: t_{66} = 5.90, p < .0001; UVT-A: t_{68} = 3.14, p = .0013). A significant reduction in RT associated with an increase in mutual information was also found in both tasks (UVT-V: reduction = 43.8 ± 5.1 ms, t_{66} = 5.35, p < .0001; UVT-A: reduction = 43.3 ± 6.7 ms, t_{68} = 2.43, p = .0009). The total uncertainty after information reduction in the Alternating block compared to the Balanced block was 0.50 bit for the UVT-V and 0.56 bit for the UVT-A based on the empirical data, indicating that the estimated reduction of uncertainty of context was actually less than the estimated 1 bit of mutual information, which might be due to the cost of control of the motor response in the alternating condition.

3.2. Involvement of the CCN in uncertainty processing: GLM results

Significant increases in activation as a function of information entropy in the UVT-V was found bilaterally in all cortical regions of the CCN except the AIC, while corresponding significant decreases in activation were found in the mid temporal gyrus and the ventral medial prefrontal cortex (Fig. 3a and Table 3). A similar effect of information entropy was revealed in the UVT-A (Fig. 3b and Table 3): there was a significant increase in activation in cortical and subcortical regions of the CCN except in the right AIC, the right FEF, and the left IPS. This effect was also found in some regions outside the CCN, including the right superior temporal gyrus and the left cerebellum (not shown in the figure). A corresponding significant decrease in activation as a function of entropy in the UVT-A was found bilaterally in the mid occipital gyrus.

Surprise was associated with significant increases in activation in all regions of the CCN bilaterally for the UVT-V and UVT-A, together with modality-specific activation increases in visual areas including the calcarine gyrus and the mid temporal gyrus for the UVT-V, and in auditory cortex including the Heschl's gyrus and the superior temporal gyrus for the UVT-A (Fig. 3c and d and Table 4).

The effect of mutual information was associated with significant decreases in activation in the left IPS, the left calcarine gyrus extending to the mid occipital gyrus, and the right supramaringal gyrus only in the UVT-V (Fig. 3e and Table 5). No significant increase or

decrease in activation associated with mutual information was found for the UVT-A (Fig. 3f).

Regional activation in each ROI is illustrated in Fig. 4, revealing a linear trend of activation increase as a function of entropy, increased activation in the high surprise condition, and decreased activation in the alternating block. Although the association between entropy and activation was not perfectly linear for some ROIs, higher-order non-linear relationships were not tested due to the lack of specific hypotheses. The regions of the CCN showed activation below 0 in most of the conditions expect the low-probability condition (i.e., the condition with the highest uncertainty in entropy or surprise).

3.3. The mediative role of the CCN in uncertainty processing: Results of the multilevel mediation analyses

Brain activation associated with the process of information conveyed by the context is showed in Fig. 5 and Table 6 for the UVT-V and in Fig. 6 and Table 7 for the UVT-A, with a similar pattern of activation for the two tasks. Significant increases in activation associated with the increase in information entropy (path *a*) was revealed in the left IPS, the right FEF, and the right postcentral gyrus in the UVT-V. This effect was also revealed in regions of the CCN including the ACC, the FEF, the left IPS, and the left and right thalamus, and in the superior temporal gyrus bilaterally in the UVT-A. These findings were consistent with the GLM results. For both tasks, significant increases in activation associated with the increase in RT, controlling for the effect of information entropy (path *b*), was revealed in all regions of the CCN bilaterally, as well as in the posterior insular cortex (PIC), the precentral and postcentral gyri, the dorsolateral prefrontal cortex (DLPFC), and visual areas including the primary visual cortex, the extrastriate areas, and the fusiform gyrus. The significant increase in activation associated with the mediation effect (top panel of the figures) was found in the FPN sub-network of the CCN in both tasks, in addition to the ACC in the UVT-A.

Brain activation associated with the processing of information conveyed by events was shown in Fig. 7 and Table 8 for the UVT-V and in Fig. 8 and Table 9 for the UVT-A. Significant increases in activation associated with the increase in surprise (path *a*) was revealed in all cortical regions of the CCN, and in the precentral and postcentral gyri for both tasks. This effect was also significant in the auditory cortex, including the Heschl's gyrus and the superior temporal gyrus for the UVT-A. For both tasks, significant increases in activation associated with the increase in RT, controlling for the effect of surprise (path *b*), was revealed bilaterally in all regions of the CCN, and in the precentral and postcentral gyri, the DLPFC, and visual areas including the primary visual cortex, extrastriate areas, and fusiform gyri. The significant increase in activation associated with the mediation effect (top panel of the figures) was observed bilaterally in all regions of the CCN except for the right AIC in both tasks, and in auditory cortex in the UVT-A.

4. Discussion

The convergent findings of supramodal involvement of the CCN in the processing of information conveyed by context and event in both visual and auditory modalities in this study provides empirical evidence supporting the information theory account of cognitive

control (Fan, 2014). Consistent with our prediction, the CCN showed an increase in activation as a function of entropy and an increase in activation in the high surprise condition compared to the low surprise condition, indicating that the CCN is an information entity for cognitive control that is generally involved in the control of the processing of information conveyed by both context and event. The significant mediation effect by the activation of the CCN in both the entropy-RT and the surprise-RT relationships further demonstrates the central role of this network in cognitive control. The common pattern of activation for both visual and auditory tasks found in this study supports the hypothesis that that the CCN processes high-level abstract information independent of the modality of sensory input.

The findings regarding the involvement of the CCN in the processing of information conveyed by an event and a context that comprises multiple events may provide new insights into the function of the CCN from the perspective of information theory. The CCN is part of the taskpositive network (Shulman et al., 1997) that is involved in a broad range of cognitive tasks, with its functional role still being debated. Uncertainty has been proposed to be one of the most important determinants of the activation of the CCN, with the level of uncertainty quantified in information entropy (for context) and in surprise (for event) based on information theory, thereby representing a measure of cognitive control load (Fan, 2014). The linear relationship between activation in regions of the CCN and the information uncertainty of a single trial has been demonstrated in our previous studies (Fan et al., 2014; Wu et al., 2018, 2020, 2019b), in which trials in the task were independent of each other. The current study, in which the probability of events in a block was parametrically manipulated, provided further evidence of a role for the CCN in encoding and processing of both individual event type in a context and the context itself. The association of the increase in activation of the CCN with both information entropy and surprise indicates that this network functions not only to coordinate mental operations to implement control for each single event, but also to process contextual information conveyed by different events in a sequence.

The current findings may inform our understanding of the functional role of the CCN in classical tasks that manipulate the probability of events or the number of choices. For example, the CCN activation typically observed using the Go/No-Go task may not only be attributable to the inhibitory processing (e.g., prepotent response inhibition), but may also be driven by the increase in surprise in the low-probability No-Go condition compared to the high-probability Go condition. Likewise, evidence of the involvement of the CCN in decision-making from studies using choice selection tasks can be attributed to the effect of entropy. The computation of entropy for n alternative choices with equal probability can be calculated as $\log_2(n)$, and monotonic increase in activation in the CCN as a function of the entropy has been observed in the current and other studies (e.g., Lee and Keller, 2008; Lee et al., 2006; Wu et al., 2018). Findings of reduced activation in the CCN for fixed sequences compared to random sequences, which purportedly support a role for this network in planning (e.g., Koechlin et al., 2000), can be interpreted as an effect of mutual information in reducing uncertainty in context with a fixed sequence. The role of the CCN in sub-domains of cognitive control (e.g., inhibition and planning) and in decision-making that involves intensive cognitive control was not directly tested in the current study, but our

previous meta-analytic study demonstrated a reliable association between CCN activation and information processing of uncertainty in these domains (Wu et al., 2019a).

The role of the CCN in mediating the entropy-RT and surprise-RT relationships further reveals how this network functions to coordinate thoughts and actions in the implementation of cognitive control. The association of CCN activation and entropy/surprise revealed in path *a* of the mediation analysis and in the GLM reflects uncertainty processing in the CCN. The slight difference between the results of path *a* and the GLM may have resulted from the difference between single-event extraction and classical GLM in detection power, as well as differences in thresholding (see Wu et al., 2018). The association between CCN activation and RT when controlling for entropy/surprise found in path *b* demonstrated that the CCN also contributes to response generation. Importantly, the finding of the CCN as a mediator of the entropy/surprise-RT relationship demonstrated the central role of the CCN in bridging uncertainty representation and behavioral response by processing uncertainty to map inputs to corresponding outputs under the guidance of the current goal.

Activation increased as a function of entropy in the FPN for both the visual and auditory tasks, while this relationship was only seen in the ACC of the CON in the auditory task. These patterns were consistent with our previous study that revealed a steeper slope for the entropy-activation linear relationship in the FPN than the CON (Fan et al., 2014), indicating that the FPN was recruited heavily when there was an increase in the amount of information conveyed by context. In contrast, the effect of surprise was observed in all regions of the CCN in both tasks, suggesting that both sub-networks were recruited heavily for the processing of information conveyed by events. However, this difference may be due to the greater range of uncertainty increase in the contrast for surprise ($3 - 0.19 = 2.81$ bits) than in the contrast for entropy ($1 - 0 = 1$ bit), which may result in the recruitment of additional regions of the CCN to ensure efficient control. In addition, the activation decrease in the IPS of the FPN associated with an increase in mutual information (less uncertain) in the visual task suggests that this region may play a specific role in the processing of the context of a sequence with events presented in random order in contrast to a fixed order in the visual modality.

The finding that activation in regions of the CCN was below baseline in most of the conditions and was above baseline only in conditions with high levels of uncertainty (i.e., the low-probability condition for all regions in both tasks and the balanced condition for the FEF and IPS in the UVT-V) indicates that this activation reflects the difference between uncertainty associated with particular task conditions and state uncertainty (i.e., uncertainty during the fixation period prior to target onset) (Bach et al., 2009; Fan et al., 2014). The state uncertainty was approximately 3 bits during the anticipation of the potential stimulus location/frequency (8 possible locations/frequencies in the UVT; $\log2(8) = 3$ bits), but was reduced to 0 bit after the target onset because this state uncertainty no longer existed. Therefore, these below zero parameter estimates in the CCN may reflect a decline in the total amount of uncertainty compared to baseline uncertainty. This pattern was also consistent with our previous study that revealed deactivation in the CCN in low entropy conditions (Fan et al., 2014).

Information processing in the brain recruits both modality-general regions (i.e., the CCN) and modality-specific sensory regions (e.g., the auditory cortex). The CCN was involved in both uncertainty representation and processing (path *a*) and response generation (path *b*) as well as in the coordination of these two stages (the mediation effect) for the processing of information conveyed by both context and event. These findings point to a central role of the CCN in uncertainty processing. In contrast, modality-specific sensory regions only showed a significant involvement in representation and processing of uncertainty in information conveyed by events, but not information conveyed by the context. These findings suggest that representation and processing uncertainty for single event incorporates both modality-specific and modality-general processes that require coupling between sensory regions and the CCN. In contrast, the representation and processing of uncertainty in a context involves higher-level abstract information that is independent of the modality of input, and thus does not necessitate the recruitment of modality-specific sensory regions. In addition, auditory areas showed a significant mediation effect in the UVT-A, but visual areas did not show such an effect in the UVT-V, suggesting that auditory cortex may also plays a central role in controlling the processing of information conveyed by events received in the auditory modality. A future study with within-subject comparisons of the cognitive control of information received from the visual and auditory modalities would offer solid evidence for a supra-modal role of the CCN in the processing of information conveyed by context and event. Brain regions besides the CCN and sensory regions may also contribute to uncertainty processing. For example, regions in the cerebellum showed an increase in activation as a function of uncertainty associated with context and event, which is consistent with a large literature showing a broad involvement of the cerebellum in cognitive control (Bellebaum and Daum, 2007; Bostan et al., 2013; Niendam et al., 2012; Schweizer et al., 2007).

The current study provides systematic insight into the role of the CCN in the processing of information conveyed by context and event that supports the hypothesis that the CCN is a high-level information processing entity in the brain. Computations of uncertainty are based on estimations of the probabilities of occurrence of different event types. The brain has to continuously update subjective internal representations of the experienced event and context. Therefore, uncertainty processing executed by the CCN may involve a subjective and dynamic mechanism. These results shed light on the theories of higher-level cognitive domains, such as decision-making and statistical learning (Alexandre et al., 2019; Siegelman et al., 2019), and advance the methods available to assess the deficit in cognitive control in patients with neuropsychiatric disorders (Mackie and Fan, 2016; Silverstein et al., 2017).

Acknowledgments

References

Alexandre Z, Oleg S, Giovanni P, 2019. An information-theoretic perspective on the costs of cognition. Neuropsychologia 123, 5–18. [PubMed: 30268880]

Atlas LY, Bolger N, Lindquist MA, Wager TD, 2010. Brain mediators of predictive cue effects on perceived pain. J. Neurosci 30, 12964–12977. [PubMed: 20881115]

Atlas LY, Lindquist MA, Bolger N, Wager TD, 2014. Brain mediators of the effects of noxious heat on pain. Pain 155, 1632–1648. [PubMed: 24845572]

Bach DR, Seymour B, Dolan RJ, 2009. Neural activity associated with the passive prediction of ambiguity and risk for aversive events. J. Neurosci 29, 1648–1656. [PubMed: 19211872]

Bellebaum C, Daum I, 2007. Cerebellar involvement in executive control. Cerebellum 6, 184–192. [PubMed: 17786814]

Bostan AC, Dum RP, Strick PL, 2013. Cerebellar networks with the cerebral cortex and basal ganglia. Trends Cognit. Sci 17, 241–254. [PubMed: 23579055]

Botvinick M, Nystrom LE, Fissell K, Carter CS, Cohen JD, 1999. Conflict monitoring versus selection-for-action in anterior cingulate cortex. Nature 402, 179. [PubMed: 10647008]

Botvinick MM, Braver TS, Barch DM, Carter CS, Cohen JD, 2001. Conflict monitoring and cognitive control. Psychol. Rev 108, 624. [PubMed: 11488380]

Braver TS, Barch DM, Gray JR, Molfese DL, Snyder A, 2001. Anterior cingulate cortex and response conflict: effects of frequency, inhibition and errors. Cereb. Cortex 11, 825–836. [PubMed: 11532888]

Cai W, Ryali S, Chen T, Li CS, Menon V, 2014. Dissociable roles of right inferior frontal cortex and anterior insula in inhibitory control: evidence from intrinsic and task-related functional parcellation, connectivity, and response profile analyses across multiple datasets. J. Neurosci 34, 14652–14667. [PubMed: 25355218]

Carter CS, Braver TS, Barch DM, Botvinick MM, Noll D, Cohen JD, 1998. Anterior cingulate cortex, error detection, and the online monitoring of performance. Science 280, 747–749. [PubMed: 9563953]

Carter CS, Macdonald AM, Botvinick M, Ross LL, Stenger VA, Noll D, Cohen JD, 2000. Parsing executive processes: strategic vs. evaluative functions of the anterior cingulate cortex. Proc. Natl. Acad. Sci 97, 1944–1948. [PubMed: 10677559]

Choi JM, Padmala S, Pessoa L, 2012. Impact of state anxiety on the interaction between threat monitoring and cognition. Neuroimage 59, 1912–1923. [PubMed: 21939773]

Corbetta M, 1998. Frontoparietal cortical networks for directing attention and the eye to visual locations: Identical, i ndependent, or overlapping neural systems? Proc. Natl. Acad. Sci. USA 95, 831–838. [PubMed: 9448248]

Cousineau D, 2005. Confidence intervals in within-subject designs: a simpler solution to Loftus and Masson's method. Tutor. Quant. Methods Psychol 1, 42–45.

Derrfuss J, Brass M, Neumann J, von Cramon DY, 2005. Involvement of the inferior frontal junction in cognitive control: meta-analyses of switching and Stroop studies. Hum. Brain Mapp 25, 22–34. [PubMed: 15846824]

Dosenbach NU, Fair DA, Cohen AL, Schlaggar BL, Petersen SE, 2008. A dual-networks architecture of top-down control. Trends Cognit. Sci 12, 99–105. [PubMed: 18262825]

Dosenbach NU, Fair DA, Miezin FM, Cohen AL, Wenger KK, Dosenbach RA, Fox MD, Snyder AZ, Vincent JL, Raichle ME, 2007. Distinct brain networks for adaptive and stable task control in humans. Proc. Natl. Acad. Sci. USA 104, 11073–11078. [PubMed: 17576922]

Fan J, 2014. An information theory account of cognitive control. Front. Hum. Neurosci 8, 680. [PubMed: 25228875]

Fan J, Flombaum J, McCandliss BD, Thomas KM, Posner MI, 2003. Cognitive and brain consequences of conflict. Neuroimage 18, 42–57. [PubMed: 12507442]

Fan J, Van Dam NT, Gu X, Liu X, Wang H, Tang CY, Hof PR, 2014. Quantitative characterization of functional anatomical contributions to cognitive control under uncertainty. J. Cognit. Neurosci 26, 1490–1506. [PubMed: 24392900]

Friston KJ, Fletcher P, Josephs O, Holmes A, Rugg M, Turner R, 1998. Event-related fMRI: characterizing differential responses. Neuroimage 7, 30–40. [PubMed: 9500830]

Friston KJ, Williams S, Howard R, Frackowiak RS, Turner R, 1996. Movement-related effects in fMRI time-series. Magn. Reson. Med 35, 346–355. [PubMed: 8699946]

Friston KJ, Worsley KJ, Frackowiak RS, Mazziotta JC, Evans AC, 1994. Assessing the significance of focal activations using their spatial extent. Hum. Brain Mapp 1, 210–220. [PubMed: 24578041]

Harrison LM, Duggins A, Friston KJ, 2006. Encoding uncertainty in the hippocampus. Neural Netw. 19, 535–546. [PubMed: 16527453]

Hick WE, 1952. On the rate of gain of information. Q. J. Exp. Psychol 4, 11–26.

Hyman R, 1953. Stimulus information as a determinant of reaction time. J. Exp. Psychol 45, 188. [PubMed: 13052851]

Kinnison J, Padmala S, Choi J-M, Pessoa L, 2012. Network analysis reveals increased integration during emotional and motivational processing. J. Neurosci 32, 8361–8372. [PubMed: 22699916]

Koechlin E, Corrado G, Pietrini P, Grafman J, 2000. Dissociating the role of the medial and lateral anterior prefrontal cortex in human planning. Proc. Natl. Acad. Sci 97, 7651–7656. [PubMed: 10852964]

Koziol LF, 2014. Cognitive control, reward, and the basal ganglia. The Myth of Executive Functioning. Springer, pp. 61–64.

Lau H, Rogers RD, Passingham RE, 2006. Dissociating response selection and conflict in the medial frontal surface. NeuroImage 29, 446–451. [PubMed: 16150611]

Lee K-M, Keller EL, 2008. Neural activity in the frontal eye fields modulated by the number of alternatives in target choice. J. Neurosci 28, 2242–2251. [PubMed: 18305257]

Lee K-M, Wade AR, Lee B-T, 2006. Differential correlation of frontal and parietal activity with the number of alternatives for cued choice saccades. NeuroImage 33, 307–315. [PubMed: 16919481]

Luks TL, Simpson GV, Dale CL, Hough MG, 2007. Preparatory allocation of attention and adjustments in conflict processing. NeuroImage 35, 949–958. [PubMed: 17258912]

MacDonald AW, Cohen JD, Stenger VA, Carter CS, 2000. Dissociating the role of the dorsolateral prefrontal and anterior cingulate cortex in cognitive control. Science 288, 1835–1838. [PubMed: 10846167]

Mackie MA, Fan J, 2016. Reduced efficiency and capacity of cognitive control i n autism spectrum disorder. Autism Res. 9, 403–414. [PubMed: 26171787]

MacKinnon DP, Krull JL, Lockwood CM, 2000. Equivalence of the mediation, confounding and suppression effect. Prevent. Sci 1, 173–181.

Miller EK, Cohen JD, 2001. An integrative theory of prefrontal cortex function. Annu. Rev. Neurosci 24, 167–202. [PubMed: 11283309]

Nastase S, Iacovella V, Hasson U, 2014. Uncertainty in visual and auditory series is coded by modality-general and modality-specific neural systems. Hum. Brain Mapp 35, 1111–1128. [PubMed: 23408389]

Nee DE, Wager TD, Jonides J, 2007. Interference resolution: insights from a meta-analysis of neuroimaging tasks. Cognit. Affect. Behav. Neurosci 7, 1–17. [PubMed: 17598730]

Niendam TA, Laird AR, Ray KL, Dean YM, Glahn DC, Carter CS, 2012. Meta-analytic evidence for a superordinate cognitive control network subserving diverse executive functions. Cognit. Affect. Behav. Neurosci 12, 241–268. [PubMed: 22282036]

Posner M, Snyder C, 1975. Attention and cognitive control. Information Processing and Cognition: the Loyola Symposium. Erlbaum, Hillsdale NJ.

Posner MI, DiGirolamo GJ, 1998. Executive attention: conflict, target detection, and cognitive control. In: Parasuraman R (Ed.), The attentive brain. The MIT Press, pp. 401–423.

Rissman J, Gazzaley A, D'esposito M, 2004. Measuring functional connectivity during distinct stages of a cognitive task. NeuroImage 23, 752–763. [PubMed: 15488425]

Rossi AF, Pessoa L, Desimone R, Ungerleider LG, 2009. The prefrontal cortex and the executive control of attention. Exp. Brain Res 192, 489–497. [PubMed: 19030851]

Schweizer TA, Oriet C, Meiran N, Alexander MP, Cusimano M, Stuss DT, 2007. The cerebellum mediates conflict resolution. J. Cognit. Neurosci 19, 1974–1982. [PubMed: 17892387]

Shannon CE, Weaver W, 1949. The Mathematical Theory of Communication. University of Illinois Press, Urbana, p. 5.

Shulman GL, Fiez JA, Corbetta M, Buckner RL, Miezin FM, Raichle ME, Petersen SE, 1997. Common blood flow changes across visual tasks: II. Decreases in cerebral cortex. J. Cognit. Neurosci 9, 648–663. [PubMed: 23965122]

Siegelman N, Bogaerts L, Frost R, 2019. What determines visual statistical learning performance? Insights from information theory. Cognit. Sci 43, e12803. [PubMed: 31858628]

Silverstein SM, Wibral M, Phillips WA, 2017. Implications of information theory for computational modeling of schizophrenia. Comput. Psychiatry 1, 82–101.

Spagna A, Mackie M-A, Fan J, 2015. Supramodal executive control of attention. Front. Psychol 6, 65. [PubMed: 25759674]

Spagna A, Wu T, Kim K, Fan J, 2020. Supramodal executive control of attention: Evidence from unimodal and crossmodal dual conflict effects. Cortex 133, 266–276. [PubMed: 33157346]

Strange BA, Duggins A, Penny W, Dolan RJ, Friston KJ, 2005. Information theory, novelty and hippocampal responses: unpredicted or unpredictable? Neural Netw. 18, 225–230. [PubMed: 15896570]

Wager TD, Davidson ML, Hughes BL, Lindquist MA, Ochsner KN, 2008. Prefrontal-subcortical pathways mediating successful emotion regulation. Neuron 59, 1037–1050. [PubMed: 18817740]

Wager TD, Waugh CE, Lindquist M, Noll DC, Fredrickson BL, Taylor SF, 2009. Brain mediators of cardiovascular responses to social threat: part I: reciprocal dorsal and ventral sub-regions of the medial prefrontal cortex and heart-rate reactivity. NeuroImage 47, 821–835. [PubMed: 19465137]

Wu T, Chen C, Spagna A, Mackie M-A, Russell-Giller S, Xu P, Luo Y.-j., Liu X, Hof PR, Fan J, 2019a. The functional anatomy of cognitive control: a domain-general brain network for uncertainty processing. J. Comp. Neurol 528, 1265–1292. [PubMed: 31674015]

Wu T, Dufford AJ, Egan LJ, Mackie M-A, Chen C, Yuan C, Chen C, Li X, Liu X, Hof PR, Fan J, 2018. Hick–Hyman law is mediated by the cognitive control network in the brain. Cereb. Cortex 28, 2267–2282. [PubMed: 28531252]

Wu T, Spagna A, Chen C, Schulz KP, Hof PR, Fan J, 2020. Supramodal mechanisms of the cognitive control network in uncertainty processing. Cereb. Cortex 30, 6336–6349. [PubMed: 32734281]

Wu T, Wang X, Wu Q, Spagna A, Yang J, Yuan C, Wu Y, Gao Z, Hof PR, Fan J, 2019b. Anterior insular cortex is a bottleneck of cognitive control. NeuroImage 195, 490–504. [PubMed: 30798012]
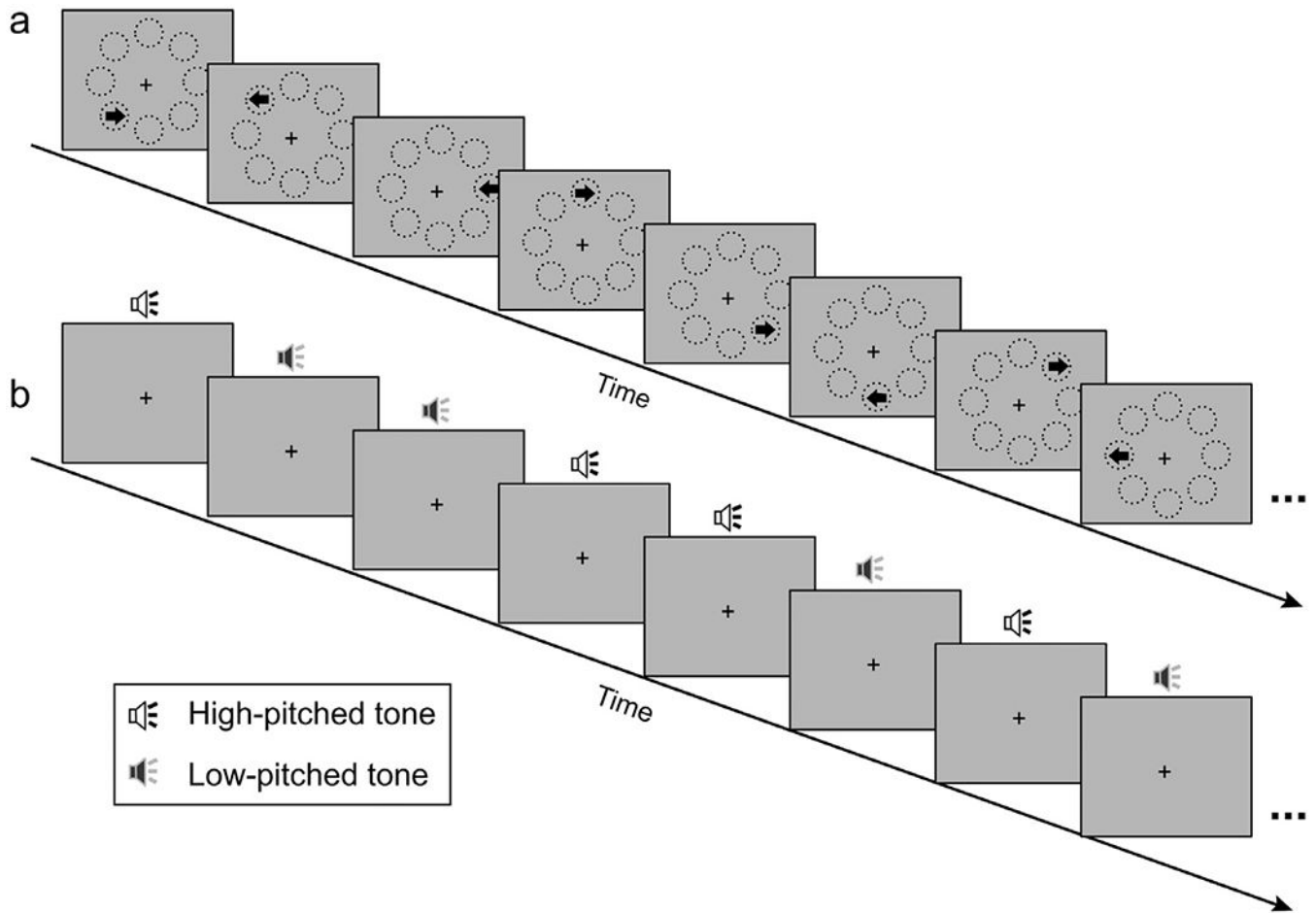
Fig. 1. Uncertainty Variation Tasks.
(a) Schematic of a partial sequence (8 of 24 stimuli) in the Balanced block of the Uncertainty Variation Task – Visual (UVT-V). Participants were required to indicate the arrow direction (left-pointing or right-pointing). (b) Schematic of a partial sequence (8 of 24 stimuli) in the Balanced block of the Uncertainty Variation Task – Auditory (UVT-A). Participants were required to indicate whether that tone is a low-pitched or a high-pitched tone. Fixation periods between the stimuli were omitted in this illustration.
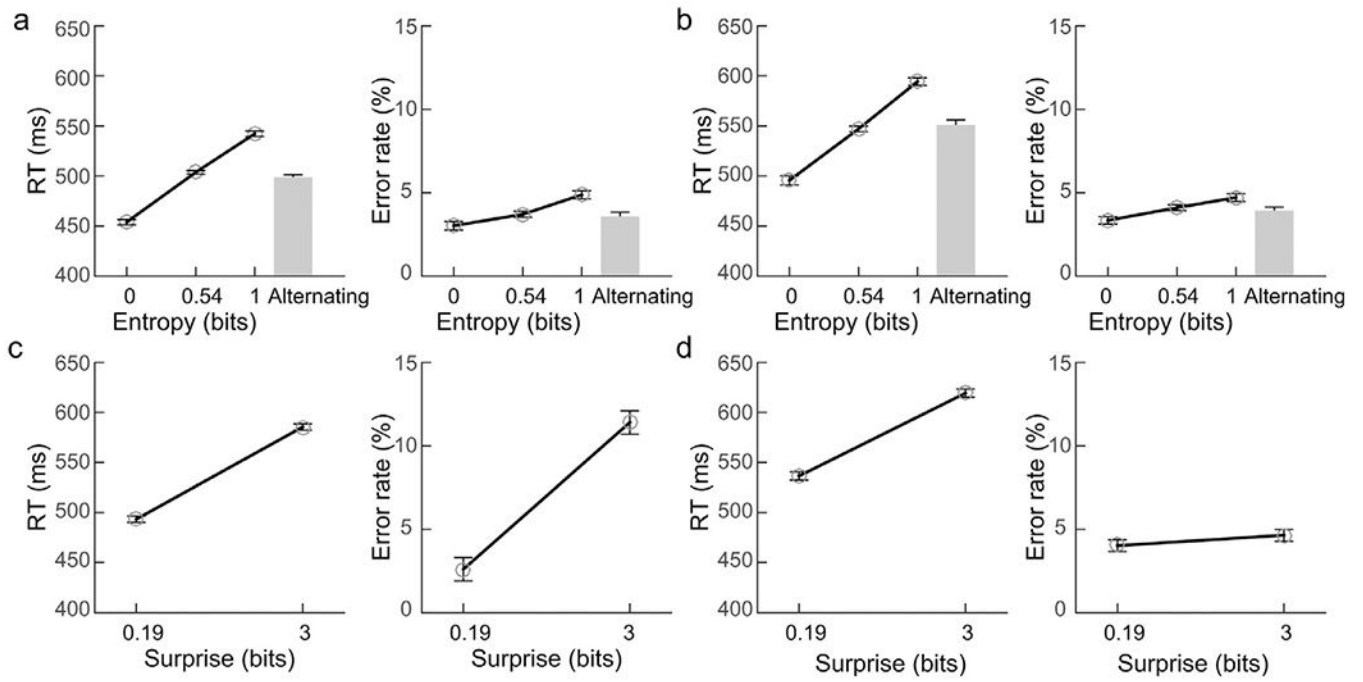
Fig. 2. Behavioral results.

Reaction time (RT) and error rate as a function of entropy in (a) UVT-V and (b) UVT-A. Entropy values were 0, 0.54, and 1 bit corresponding to the Constant, Unbalanced, and Balanced blocks, respectively. RT and error rate as a function of surprise in the (c) UVT-V and (d) UVT-A. Surprise values were 0.19 and 3 bits corresponding to the high-probability and low-probability conditions, respectively. Error bars denote the standard error in within-subject design.
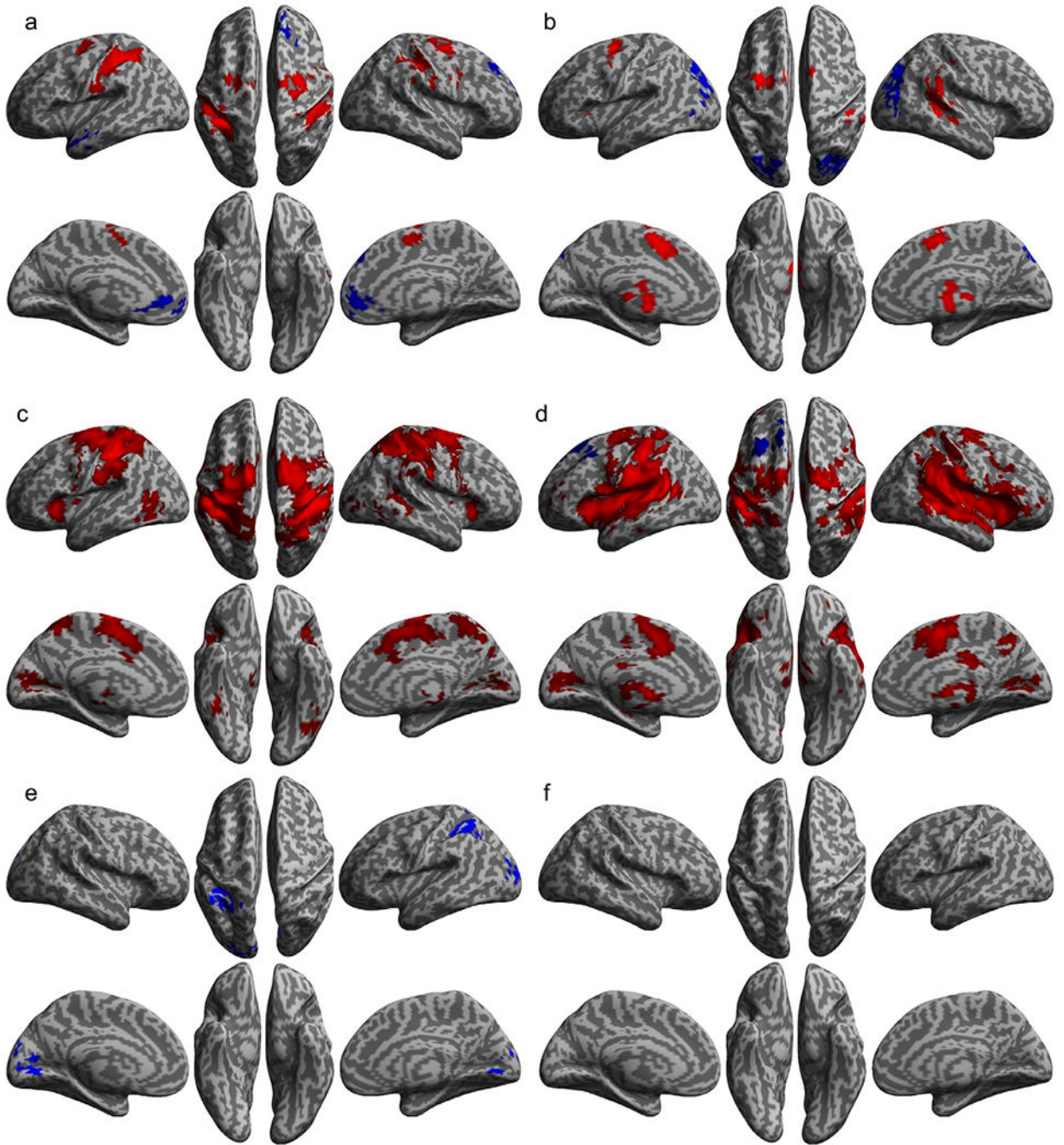
Fig. 3. Brain regions showing significant activation change as a function of uncertainty.
Regions with significant activation increase (red) or decrease (blue) as linear function of entropy in (a) UVT-V and (b) UVT-A. Regions with significant activation increase (red) or decrease (blue) as a function of surprise in (c) UVT-V and (d) UVT-A. Brain regions showing significant activation decrease associated with information reduction due to mutual information in (e) UVT-V and (f) UVT-A.
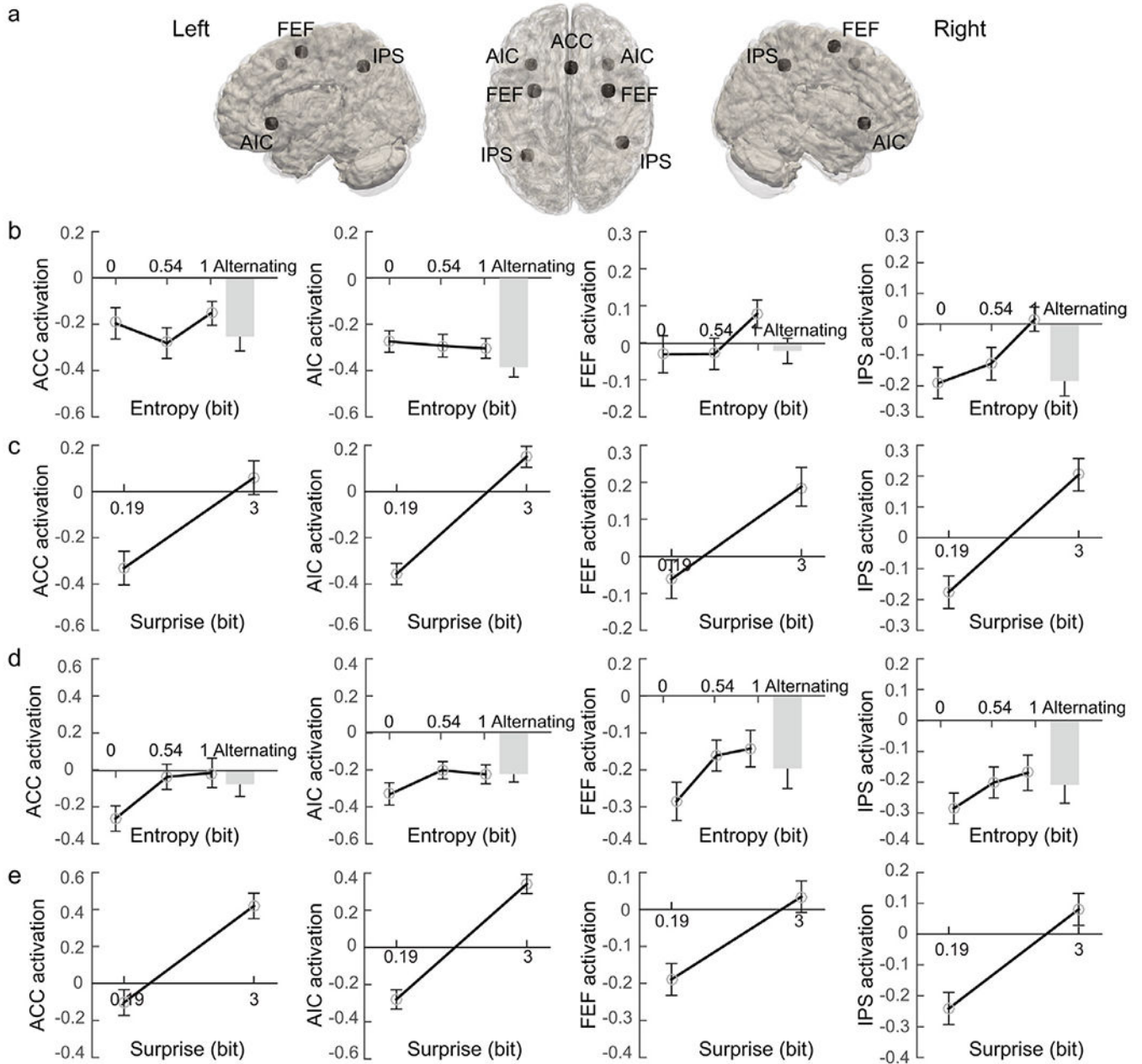
Fig. 4. Regional activation in each ROI.
(a) Localization of the ROIs in the brain. ACC: anterior cingulate cortex. AIC: anterior insular cortex. FEF: frontal eye field. IPS: areas near and along the intra-parietal sulcus. ROI activation as a function of (b) entropy and (c) surprise in the UVT-V and as a function of (d) entropy and (e) surprise in the UVT-A. Entropy values 0, 0.54, and 1 bit correspond to the Constant, Unbalanced, and Balanced blocks, respectively. Surprise values 0.19 and 3 bit correspond to the low-probability and high-probability conditions, respectively. Error bars denote the standard error in within-subject design.
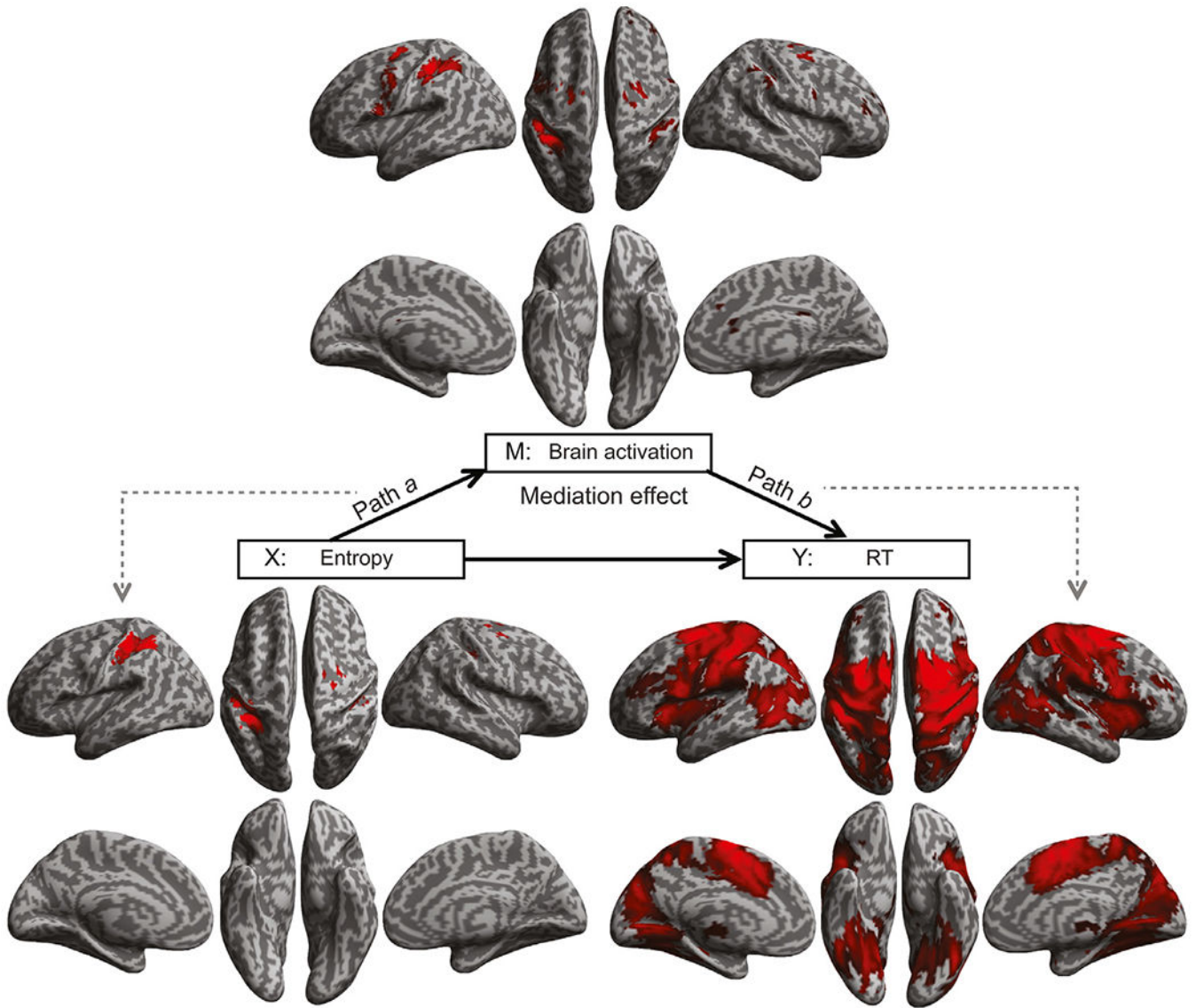
Fig. 5. Results of the mediation analysis for the entropy-RT relationship in the UVT-V.
Path *a*: association between entropy and brain activation (X to M). Path *b*: association between brain activation and RT (M to Y). Mediation effect (top panel): association between entropy and RT that can be explained by brain activation (X to M to Y).
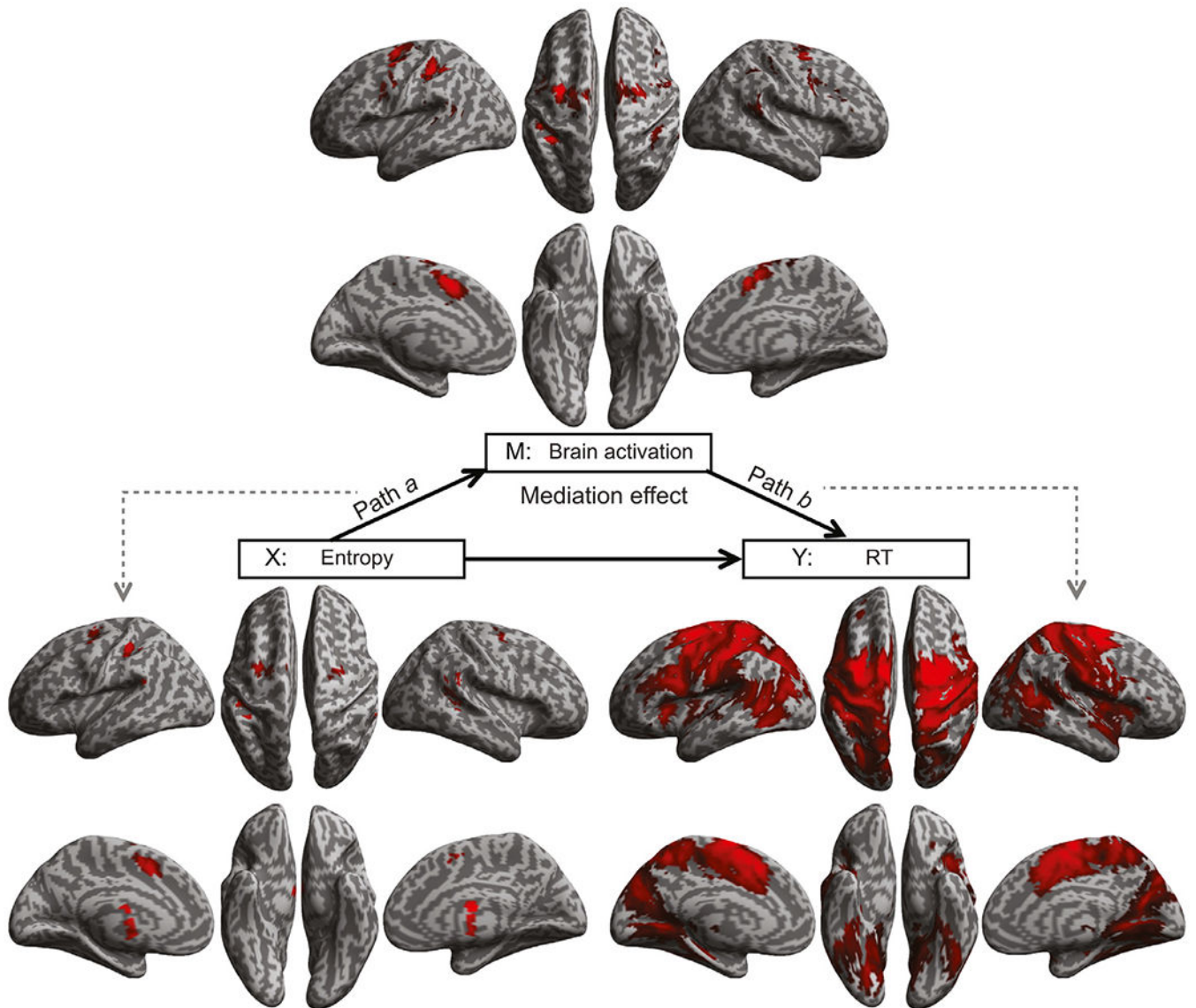
Fig. 6. Results of the mediation analysis for the entropy-RT relationship in the UVT-A.
Path *a*: association between entropy and brain activation (X to M). Path *b*: association between brain activation and RT (M to Y). Mediation effect (top panel): association between entropy and RT that can be explained by brain activation (X to M to Y).
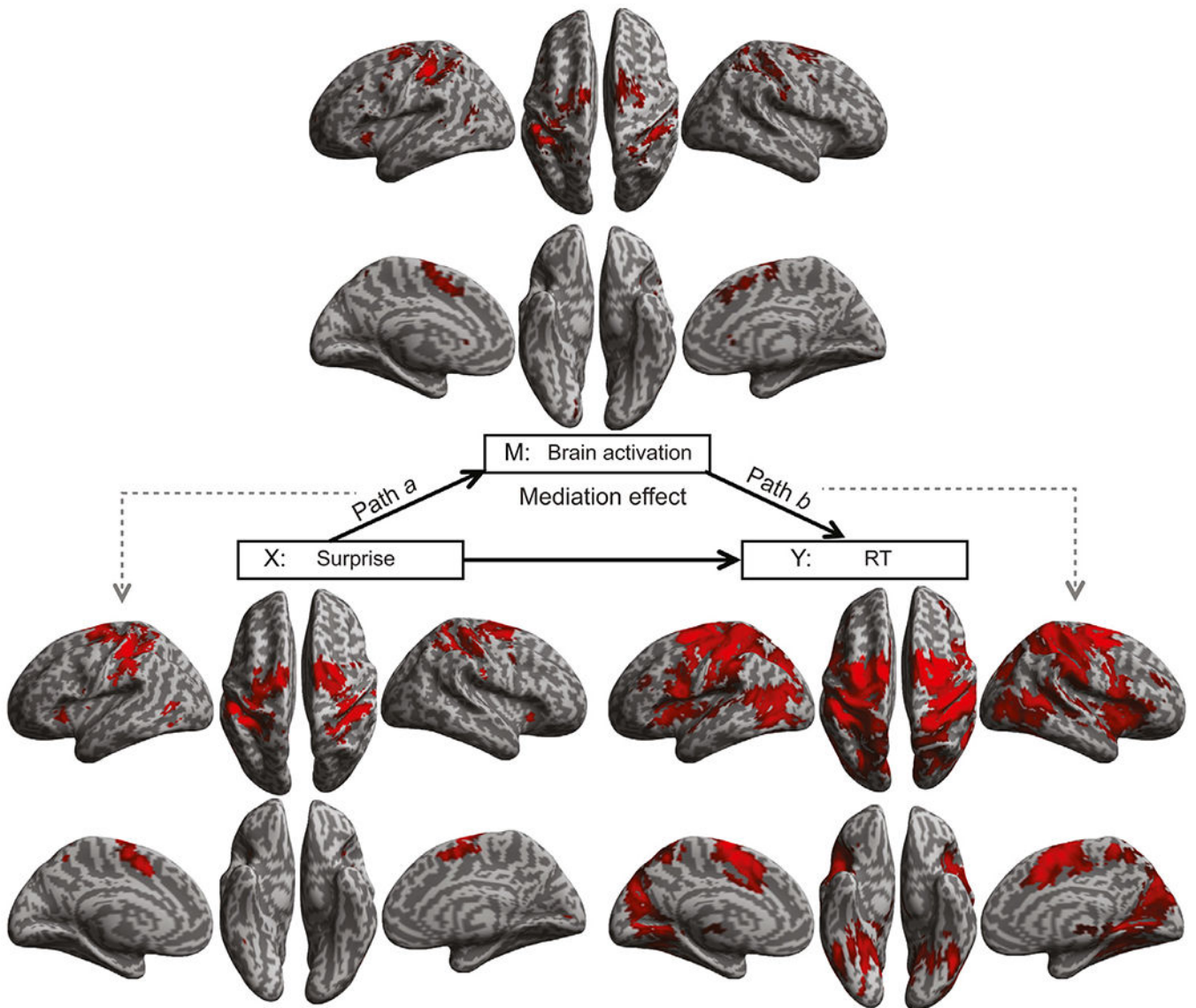
Fig. 7. Results of the mediation analysis for the surprise-RT relationship in the UVT-V.
Path *a*: association between surprise and brain activation (X to M). Path *b*: association between brain activation and RT (M to Y). Mediation effect (top panel): association between surprise and RT that can be explained by brain activation (X to M to Y).
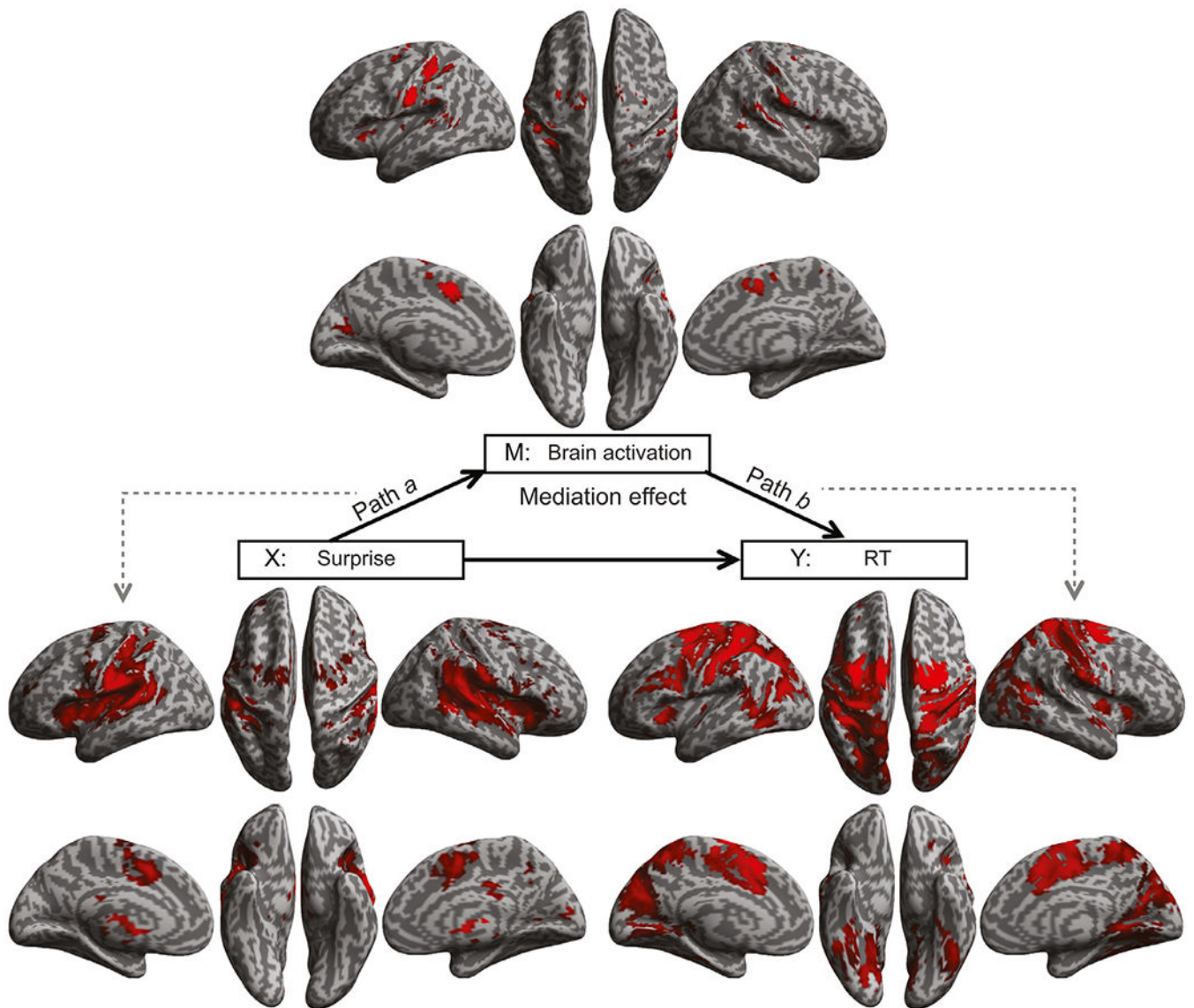
Fig. 8. Results of the mediation analysis for the surprise RT relationship in the UVT-A.
Path *a*: association between surprise and brain activation (X to M). Path *b*: association between brain activation and RT (M to Y). Mediation effect (top panel): association between surprise and RT that can be explained by brain activation (X to M to Y).

Table 1

Stimulus sequence examples, frequency of event type, and information amount for the task condition included for the analysis [a].

Block type	Stimulus sequence	Frequency	Information amount (bit)		
			Entropy	Surprise	Mutual information
Constant	LLLLLLL…	100% vs. 0%	0		
Alternating	LRLRLRLR…	50% vs. 50%	0[b]		1[c]
Unbalanced	LLLLLLRL…	87.5% vs. 12.5%	0.54	0.19 vs. 3	
Balanced	LRRLRRLL…	50% vs. 50%	1		0

Note:

[a] Only 8 out of the 24 stimuli in each block in the UVT-V are illustrated in this table.

[b,c] See Methods and Results for the estimation of the values of entropy and mutual information. L: left-pointing arrow; R: right-pointing arrow. The corresponding stimuli types in the UVT-A were high-pitched and low-pitched tones. Information amount is only listed under the conditions included in the examination of the effect of each measure of uncertainty.

Table 2

Mean ± standard deviation (SD) of reaction time (RT) and error rate in each task condition.

	Constant	Alternating	Unbalanced		Balanced
			High-probability	Low-probability	
UVT-V					
RT (ms)	454 ± 51	498 ± 58	493 ± 51	586 ± 75	542 ± 61
Error rate (%)	3.0 ± 4.0	3.6 ± 4.1	2.5 ± 3.2	11.4 ± 8.4	4.9 ± 4.4
UVT-A					
RT (ms)	496 ± 103	551 ± 118	536 ± 104	619 ± 117	594 ± 105
Error rate (%)	3.3 ± 3.4	3.9 ± 4.1	4.0 ± 3.9	4.7 ± 5.6	4.7 ± 3.9

Table 3

Brain regions with a significant change in activation associated with an increase in information entropy.

Regions	L/R	BA	x	y	z	T	Z	K
UVT-V: Increased								
Inferior parietal lobule	L	7/40	−32	−40	46	6.34	5.09	2776
Postcentral gyrus	L	3	−54	−16	18	3.24	3.00	
Inferior parietal lobule	R	7/40	40	−28	36	4.75	4.12	1562
Postcentral gyrus	R	3	30	−42	70	3.25	3.00	
Supramarginal gyrus	R	40	58	−16	22	3.00	2.80	
Superior frontal gyrus [a]	R	6/8	30	−4	62	4.03	3.61	2208
Superior frontal gyrus [a]	L	6/8	−24	−6	50	3.77	3.41	
Supplementary motor areas [b]	R	6	4	0	52	3.65	3.32	
UVT-V: Decreased								
Mid temporal gyrus	L	21	−40	6	−28	4.36	3.84	540
Orbitofrontal area	L	11	−4	48	−6	3.92	3.52	1703
Superior frontal gyrus (medial)	R	9/10	24	34	42	3.37	3.10	
UVT-A: Increased								
Superior frontal gyrus [a]	L	6/8	−24	−8	52	5.72	4.75	1799
Supplementary motor areas [b]	L	6/23	−6	8	46	4.69	4.09	
Thalamus	R		8	−2	16	4.84	4.19	3010
Anterior insular cortex [c]	L		−24	18	0	3.54	3.25	
Putamen	R		20	6	2	3.52	3.23	
Thalamus	L		−14	−16	16	3.33	3.07	
Inferior parietal lobule [d]	L	2/40	−42	−32	44	5.16	4.40	467
Superior temporal gyrus	R	20	52	−40	4	4.55	3.99	1560
Inferior parietal lobule	R	2/40	42	−30	42	3.76	3.41	
Cerebellum VI	L		−24	−52	−26	4.10	3.67	469
UVT-A: Decreased								
Mid occipital gyrus	R	19	40	−80	26	4.88	4.22	1480
Mid occipital gyrus	L	19	−32	−82	16	3.27	3.03	1215

Note: Regions are listed in a descending order by their peak Z value. For a cluster with multiple local peaks, the number of voxels in the whole cluster was only listed under the first local peak (also for other activation tables). The threshold was $p < 0.01$ ($T > 2.44$) for the height and a minimum voxel in each cluster ($k > 440$ for the UVT-V and $k > 450$ for the UVT-A) for the extent, resulting in a corrected threshold of cluster level $p < 0.05$.

L: left; R: right. BA: Brodmann area.

[a] Composing the frontal eye field (FEF).

[b] Extending to the anterior cingulate cortex (ACC).

[c] Extending to the putamen.

[d] Extending to the postcentral gyrus.

Table 4

Brain regions with increased activation associated with an increase in information surprise.

Regions	L/R	BA	x	y	z	T	Z	K
UVT-V: Increased (low-probability > high-probability)								
Postcentral gyrus	R	2	42	−28	42	9.17	Inf	25189
Postcentral gyrus	L	2	−40	−32	48	7.61	7.12	
Superior frontal gyrus [a]	L	6/8	−16	−6	66	6.39	6.09	
Anterior insular cortex	L		−30	22	4	5.93	5.69	
Inferior parietal lobule	R	7/40	30	−44	62	5.58	5.37	
Superior frontal gyrus [a]	R	6/8	14	−2	66	5.53	5.32	
Anterior insular cortex	R		32	22	−2	5.48	5.28	
Rolandic operculum	L		−44	−2	10	5.12	4.96	
Postcentral gyrus	L	3	−54	−22	26	4.85	4.70	
Precuneus	R	7	14	−60	46	4.31	4.20	
Anterior cingulate cortex	R	32	10	16	36	3.75	3.68	
Mid temporal gyrus	R	21	54	−42	−4	3.61	3.54	
Cerebellum VI	R		36	−44	−28	5.13	4.96	1124
Cerebellum IV & V	R		14	−52	−16	3.62	3.55	
Cerebellum VI	L		−34	−42	−34	4.76	4.62	1758
Mid temporal gyrus	L	21	−46	−64	4	4.50	4.38	
Thalamus	L		−16	−20	12	4.56	4.45	1807
Thalamus	R		14	−18	12	4.04	3.95	
Calcarine gyrus	L	17	−8	−82	10	4.10	4.01	1782
UVT-A: Increased (low-probability > high-probability)								
Superior temporal gyrus	L	21	−54	−40	16	8.31	7.70	49887
Mid temporal gyrus [b]	R	21	54	−38	8	7.49	7.03	
Superior temporal gyrus	R	20	54	−16	−2	7.01	6.62	
Inferior parietal lobule [c]	L	2/7	−42	−32	42	6.82	6.46	
Heschl's gyrus	L	42	−38	−18	8	6.57	6.25	
Anterior insular cortex	L		−32	14	0	6.28	6.00	
Anterior insular cortex	R		28	20	−10	6.15	5.89	
Supplementary motor area [d]	R	6/32	6	−2	52	5.98	5.73	
Thalamus	L		−4	−6	0	5.68	5.47	
Superior frontal gyrus [a]	L	6/8	−24	−10	54	5.20	5.03	
Superior temporal pole	R	38	48	4	−16	5.16	5.00	
Thalamus	R		18	−22	10	5.13	4.97	
Inferior parietal lobule	R	2/7	44	−32	46	4.77	4.64	
Precentral gyrus	L	4	−56	4	16	4.34	4.24	
Precuneus	R	7	12	−50	42	4.24	4.14	
Cerebellum VI & V	R		20	−40	−28	4.20	4.10	

Regions	L/R	BA	x	y	z	T	Z	K
Vermis VI & V		5	−2	−52	−20	4.17	4.08	
Calcarine gyrus	L	17	−14	−78	10	3.94	3.86	
Postcentral gyrus	R		22	−46	66	3.91	3.84	
Cerebellum VI & V	L		−26	−42	−28	3.89	3.81	
Mid temporal gyrus	L	21	−50	−34	−10	3.78	3.71	
Cerebellum VIII	R		20	−62	−42	3.73	3.66	
Precentral gyrus	L		−50	−6	38	3.71	3.65	
Inferior frontal gyrus	R	44	36	14	30	3.70	3.63	
Angular gyrus	R	40	56	−52	38	3.58	3.52	
Calcarine gyrus	R		10	−76	4	3.52	3.47	
Cerebellum crus I	L		−14	−70	−32	3.46	3.41	
UVT-A: Negative (low-probability < high-probability)								
Mid frontal gyrus	L	8	−32	20	46	4	3.92	1009

Note: The threshold was $p < 0.01$ ($T > 2.44$) for the height and a minimum voxel in each cluster ($k > 330$ for the UVT-V and $k > 415$ for the UVT-A) for the extent, resulting in a corrected threshold of cluster level $p < 0.05$.

[a]Composing the FEF.

[b]Extending to the Heschl's gyrus.

[c]Extending to the postcentral gyrus.

[d]Extending to the ACC.

Table 5

Brain regions with significant reduction of activation associated with an increase in mutual information (Alternating < Balanced) in UVT-V.

Regions	L/R	BA	x	y	z	T	Z	K
Inferior parietal lobule	L	7/40	−34	−44	38	4.61	4.02	1213
Mid occipital gyrus	L	18	−14	−98	10	4.33	3.82	1273
Calcarine gyrus	L	17	−8	−70	8	3.94	3.54	
Supramarginal gyrus	R	39	48	−40	26	3.17	2.94	358

Note: The threshold was $p < 0.01$ (T > 2.44) for the height and a minimum voxel in each cluster ($k > 295$) for the extent, resulting in a corrected threshold of cluster level $p < 0.05$.

Table 6

Brain regions with significant increase in activation in the mediation analysis for the processing of information conveyed by context (entropy) in UVT-V

Regions	L/R	BA	x	y	z	Z	K
Path a							
Inferior parietal lobule	L	7/40	−38	−48	58	0.49	1436
Superior frontal gyrus [a]	R	6/8	26	−8	70	0.33	135
Postcentral gyrus	R	2/3	42	−26	42	0.21	131
Path b							
Superior frontal gyrus [a]	L	6/8	−22	−10	54	4.44	71432
Superior frontal gyrus [a]	R	6/8	32	−14	56	4.00	
Supplementary motor area [b]	R	6/32	12	2	56	3.85	
Inferior parietal lobule	L	40	−44	−32	38	3.44	
Inferior temporal gyrus	L	21	−38	−60	−6	3.25	
Posterior insular cortex	L		−46	0	18	3.23	
Anterior insular cortex	L		−28	22	6	3.10	
Inferior occipital gyrus	R	19	42	−78	0	3.00	
Inferior parietal lobule	R	7/40	28	−42	52	2.98	
Anterior insular cortex	R		32	18	10	2.93	
Inferior parietal lobule	L	7	−26	−44	50	2.91	
Fusiform gyrus	R	37	40	−50	−10	2.84	
Mid occipital gyrus	L	19	−28	−68	28	2.70	
Superior occipital gyrus	R	19	24	−68	30	2.66	
Lingual gyrus	R	18	16	−68	2	2.56	
Supramarginal gyrus	R	40	50	−18	28	2.48	
Precentral gyrus	R	6	52	6	22	2.48	
Thalamus	R		12	−18	−2	2.40	
Lingual gyrus	L	18	−10	−76	4	2.36	
Thalamus	L		−12	−20	0	2.14	
Paracentral lobule	R	4	12	−26	50	1.93	
Superior temporal gyrus	R	22	44	−22	−4	1.75	
Cerebellum VI & V	L		−16	−50	−26	1.73	
Posterior insular cortex	R		39	−1	4	1.71	
Cerebellum VI & V	R		12	−56	−22	1.68	
Superior temporal gyrus	L	22	−46	−24	2	1.47	
Inferior frontal gyrus	L	45	−44	34	20	1.32	
Mid frontal gyrus	L	46	−40	35	24	1.29	
Mid frontal gyrus	R	46	32	42	22	1.70	399
Brainstem			−2	−26	−28	1.19	250
Mediation							
Inferior parietal lobule	L	7/40	−44	−34	46	1.04	1521

Regions	L/R	BA	x	y	z	Z	K
Superior frontal gyrus [a]	L	6/8	−22	−10	54	0.85	254
Precentral gyrus	L	6	−50	0	38	0.61	738
Superior frontal gyrus [a]	R	6/8	26	−8	62	0.55	267
Inferior parietal lobule	R	7/40	40	−32	46	0.49	451
Inferior frontal gyrus	R	44	54	8	28	0.38	105
Anterior cingulate cortex	R	32	6	30	32	0.28	110
Superior frontal gyrus (medial)	R	10	14	48	28	0.14	132

Note:

[a] Composing the FEF.

[b] Extending to the ACC.

Table 7

Brain regions with significant increase in activation in the mediation analysis for the processing of context information (entropy) in UVT-A

Regions	L/R	BA	x	y	z	Z	K
Path a							
Thalamus	R		2	−8	14	0.68	1065
Thalamus	L		−10	4	13	0.49	
Supplementary motor area [a]	L	6/32	−2	6	50	0.50	672
Superior frontal gyrus [b]	L	6/8	−28	−6	54	0.38	
Vermis III			0	−36	−14	0.45	235
Superior temporal gyrus	R	22/41/42	54	−40	8	0.43	303
Inferior parietal lobule	L	7/40	−44	−32	44	0.42	224
Superior temporal gyrus	L	22/41/42	−58	−42	20	0.42	101
Cerebellum VI	L		−36	−50	−28	0.33	133
Superior frontal gyrus [b]	R	6/8	30	−6	60	0.29	124
Path b							
Superior frontal gyrus [b]	L	6/8	−18	−8	58	5.45	58141
Superior frontal gyrus [b]	R	6/8	20	−10	58	5.22	
Supplementary motor area [a]	L	6/32	−10	12	46	4.80	
Postcentral gyrus	R	2/3	32	−28	46	4.16	
Precentral gyrus	L	6	−36	−4	36	3.98	
Inferior parietal lobule	R	7/40	25	−38	52	3.96	
Postcentral gyrus	L	2/3	−36	−34	44	3.89	
Superior occipital gyrus	L	19	−24	−66	28	3.45	
Anterior insular cortex	L		−28	20	6	3.38	
Superior parietal lobule	L	5	−18	−40	64	3.36	
Inferior parietal lobule	L	7/40	−16	−62	52	3.11	
Calcarine gyrus	R	17	24	−64	20	3.07	
Precentral gyrus	R	6	44	−2	30	2.90	
Mid temporal gyrus	R	21	48	−52	0	2.67	
Inferior temporal gyrus	L	20	−48	−56	−8	2.66	
Fusiform gyrus	R	37	38	−34	−22	2.52	
Anterior insular cortex	R		32	26	4	2.51	
Thalamus	L		−14	−22	2	2.50	
Superior temporal gyrus	R	22	52	−4	−12	2.49	
Piriform cortex	R	27	22	−40	0	2.33	
Lingual gyrus	L	18	−20	−56	−2	2.30	
Fusiform gyrus	L	37	−30	−26	−26	2.25	
Posterior insular cortex	R		36	−3	11	2.23	
Thalamus	R		10	−16	−2	2.10	

Regions	L/R	BA	x	y	z	Z	K
Posterior insular cortex	L		−34	−8	12	1.74	
Heschl's gyrus	L	41/42	−46	−35	17	1.20	
Heschl's gyrus	R	41/42	36	−28	18	1.17	
Mediation							
Superior frontal gyrus [b]	L	6/8	−28	−6	54	1.53	3030
Supplementary motor area	L	6	−6	8	48	1.45	
Superior frontal gyrus [b]	R	6/8	26	−6	60	0.78	
Precentral gyrus	L	6	−44	2	34	0.74	
Precentral gyrus	R	6	54	6	38	0.57	
Anterior cingulate cortex	R	32	12	22	38	0.21	
Inferior parietal lobule	L	7/40	−40	−34	44	1.20	653
Superior temporal gyrus	R	22	64	−42	16	0.61	229
Inferior parietal lobule	R	7/40	38	−32	46	0.56	219
Cerebellum VI	L		−20	−56	−24	0.33	131
Parecentral lobule	L	4	−2	−22	68	0.31	141

Note:

[a]Extending to the ACC.

[b]Composing the FEF.

Table 8

Brain regions with significant increase in activation in the mediation analysis for the processing of information conveyed by event (surprise) in UVT-V

Regions	L/R	BA	x	y	z	Z	K
Path a							
Inferior parietal lobule	L	40	−44	−32	44	0.29	8886
Supplementary motor area [a]	L	6/32	0	2	52	0.26	
Inferior parietal lobule	R	40	48	−28	48	0.22	
Superior frontal gyrus [b]	R	6/8	28	−2	64	0.22	
Superior frontal gyrus [b]	L	6/8	−14	−6	74	0.22	
Superior parietal lobule	R	7	30	−48	66	0.20	
Superior parietal lobule	L	7	−34	−48	60	0.18	
Mid temporal gyrus	L	21	−52	−66	−2	0.20	157
Anterior insular cortex	R		34	22	−2	0.19	156
Anterior insular cortex	L		−30	22	4	0.17	161
Rolandic operculum	R		56	−20	22	0.16	95
Thalamus	L		−12	−16	10	0.15	71
Cerebellum VI	R		36	−44	−28	0.14	96
Posterior insular cortex	L		−42	−2	10	0.14	113
Calcarine cortex	R	17	14	−86	4	0.13	58
Path b							
Superior frontal gyrus [b]	L	6/8	−18	−6	58	3.99	48151
Superior frontal gyrus [b]	R	6/8	28	−4	48	3.52	
Postcentral gyrus	R	2/3	24	−38	54	3.44	
Supramarginal gyrus	R	40	48	−26	38	3.38	
Postcentral gyrus	L	2/3	−44	−32	48	3.37	
Fusiform gyrus	L	37	−38	−60	−8	3.17	
Inferior parietal lobule	R	7/40	25	−41	60	3.16	
Precentral gyrus	L	6	−46	−2	18	3.06	
Fusiform gyrus	R	37	40	−46	−10	3.06	
Mid occipital gyrus	L	19	−28	−70	28	2.96	
Mid occipital gyrus	R	19	44	−78	2	2.78	
Supplementary motor area [a]	R	6/32	10	−10	66	2.56	
Anterior insular cortex	R		36	18	10	2.55	
Calcarine cortex	R	17	16	−80	18	2.54	
Anterior insular cortex	L		−30	16	8	2.47	
Calcarine cortex	L	17	−12	−78	4	2.46	
Anterior insular cortex	L		−29	25	4	2.46	
Inferior parietal lobule	L	7/40	−22	−48	64	2.45	
Precentral gyrus	R	6	52	4	24	2.40	

Regions	L/R	BA	x	y	z	Z	K
Superior temporal gyrus	R	22	46	−22	0	2.25	
Thalamus	R		12	−18	−2	2.24	
Anterior cingulate cortex	L	32	−12	16	34	2.04	
Thalamus	L		−14	−22	2	1.92	
Superior temporal gyrus	L	22	−54	0	−8	1.78	
Superior parietal lobule	R	7	20	−62	44	1.54	
Mid frontal gyrus	R	46	32	40	22	1.67	248
Mid frontal gyrus	L	46	−40	52	12	1.11	177
Mediation							
Postcentral gyrus	L	2/3	−44	−32	46	0.61	4578
Superior frontal gyrus [b]	L	6/8	−24	−8	54	0.34	
Anterior cingulate cortex	L	6/32	−6	10	44	0.29	
Superior frontal gyrus [b]	R	6/8	24	−6	60	0.28	
Inferior parietal lobule	L	7/40	−32	−44	64	0.24	
Precuneus	L	7	−10	−58	60	0.15	
Postcentral gyrus	R	2	44	−28	44	0.40	1554
Inferior parietal lobule	R	7/40	26	−46	66	0.31	
Anterior insular cortex	L		−30	18	0	0.26	257
Rolandic operculum	L		−48	2	8	0.20	
Precentral gyrus	L	6	−42	2	34	0.22	126
Cerebellum crus I	R		24	−76	−32	0.21	198
Mid temporal gyrus	L	21	−46	−60	6	0.19	125
Inferior frontal gyrus	L	44	−54	18	32	0.15	129

Note:

[a] Extending to the ACC.

[b] Composing the FEF.

Table 9

Brain regions with significant increase in activation in the mediation analysis for the processing of information conveyed by event (surprise) in UVT-A

Regions	L/R	BA	x	y	z	Z	K
Path a							
Superior temporal gyrus [a]	L	41/42	−58	−24	14	0.46	26770
Mid temporal gyrus	R	21	58	−40	8	0.41	
Ventral striatum	L/R		0	−4	−2	0.34	
Anterior cingulate cortex	L	32	−2	6	44	0.33	
Anterior insular cortex	L		−36	14	4	0.30	
Superior temporal gyrus [a]	R	41/42	53	−36	15	0.27	
Inferior parietal lobule [b]	L	7/40	−48	−30	44	0.26	
Thalamus	L		−10	−15	9	0.23	
Superior temporal gyrus	R	22	56	−12	0	0.23	
Inferior parietal lobule [b]	R	7/40	40	−42	60	0.20	
Caudate nucleus	R		6	3	2	0.20	
Caudate nucleus	L		−11	6	2	0.19	
Inferior parietal lobule	R	7/40	45	−35	51	0.19	
Thalamus	R		14	−13	9	0.18	
Superior frontal gyrus [c]	R	6/8	28	−14	70	0.18	
Precentral gyrus	L	6	−54	4	32	0.17	
Superior frontal gyrus [c]	L	6/8	−27	−10	57	0.15	
Inferior frontal gyrus	R	44	52	12	28	0.13	
Hippocampus	R	35	26	−12	−8	0.12	
Inferior frontal gyrus	R	45	44	34	18	0.10	
Calcarine cortex	R	17	6	−80	10	0.23	81
Posterior cingulate cortex	R	23	2	−24	30	0.22	145
Cerebellum IX	L		−8	−44	−40	0.16	334
Cerebellum IV & V	L		−16	−54	−18	0.14	
Precuneus	R	7	10	−50	42	0.15	90
Cerebellum VI	R		20	−54	−20	0.15	607
Vermis VIII			6	−66	−36	0.10	95
Path b							
Superior frontal gyrus [c]	L	6/8	−28	−6	50	5.19	35599
Superior frontal gyrus [c]	R	6/8	20	−6	60	4.79	
Inferior parietal lobule	L	7/40	−30	−34	42	4.66	
Anterior cingulate cortex	L	32	−10	12	46	4.59	
Inferior parietal lobule	R	7/40	20	−36	60	4.11	
Mid occipital gyrus	L	19	−26	−64	30	4.05	
Precentral gyrus	L	6	−36	2	28	3.93	

Regions	L/R	BA	x	y	z	Z	K
Supplementary motor area	L	6	−10	−20	58	3.67	
Postcentral gyrus	R	2/3	36	−28	42	3.66	
Calcarine cortex	R	17	24	−68	20	3.49	
Postcentral gyrus	L	3	−50	−20	32	3.42	
Anterior cingulate cortex	R	24/32	10	12	32	3.30	
Mid temporal gyrus	R	22	42	−52	14	3.23	
Precuneus	L	7	−10	−56	56	3.23	
Inferior temporal gyrus	L	20	−46	−48	−10	3.21	
Postcentral gyrus	R	2/3	62	−12	24	3.20	
Inferior temporal gyrus	R	20	48	−44	−14	3.05	
Thalamus	L		−18	−24	0	2.89	
Mid frontal gyrus	L	46	−28	42	14	2.69	
Lingual gyrus	R	18	22	−54	−2	2.62	
Mid occipital gyrus	R	19	46	−80	2	2.50	
Calcarine cortex	L	17	−14	−90	14	2.46	
Lingual gyrus	L	18	−16	−62	0	2.27	
Cerebellum IV & V	R		34	−30	−28	2.17	
Cerebellum VI	R		28	−62	−26	2.02	
Superior parietal lobule	L	7	−14	−80	48	1.90	
Anterior insular cortex	L		−28	24	−2	3.39	861
Anterior insular cortex	R		30	24	4	2.80	1080
Posterior insular cortex	R		36	−4	8	2.78	
Posterior insular cortex	L		−34	−14	2	2.11	61
Mediation							
Supplementary motor area[d]	L	6/32	−6	10	46	0.62	723
Postcentral gyrus	L	2/3	−56	−18	28	0.60	1830
Inferior parietal lobule	L	7/40	−34	−34	44	0.57	
Superior temporal gyrus	L	22	−48	−32	8	0.35	
Posterior insular cortex	L		−50	−6	4	0.25	
Supramarginal gyrus	R	40	58	−16	24	0.54	783
Superior temporal gyrus	R	42	58	−40	14	0.37	
Superior frontal gyrus[c]	L	6/8	−30	−8	52	0.41	149
Paracentral lobule	L	4	−18	−12	68	0.39	156
Postcentral gyrus	R	2/3	46	−30	50	0.39	242
Anterior insular cortex	L		−30	20	6	0.35	141
Anterior insular cortex	R		52	6	−8	0.33	389
Superior frontal gyrus[c]	R	6/8	22	−6	58	0.33	158
Mid temporal gyrus	R	21	58	−52	18	0.33	161
Calcarine cortex	L	17	−12	−68	14	0.32	219
Inferior frontal gyrus	L	44	−54	12	0	0.29	116

Note:

[a]Extending to posterior insular cortex.

[b]Extending to postcentral gyrus.

[c]Composing the FEF.

[d]Extending to the ACC.